

Annexures



E-mail: amalacancerresearch@gmail.com

Phone: 0487 2307968

Institutional Animal Ethics Committee (IAEC)

(Reg. No. 149/PO/Rc/S/1999/CPCSEA)

Amala Cancer Research Centre Society



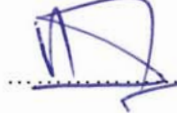
AMALANAGAR - 680 555, THRISSUR, KERALA, INDIA

Ref:

14.10.2020
Date:

Certificate

This is to certify that the project proposal no. ACRC/IAEC/20(1)-P1 entitled 'Evaluation of anticarcinogenic and chemoprotective effect of green synthesized silver nanoparticles using Curcuma rhizomes' submitted by Dr. Achuthan C R (on behalf of Ms. Aiswarya K S) has been approved/recommended by the IAEC of Amala Cancer Research Centre in its meeting dated 14.10.20 and has been sanctioned 88 Swiss albino mice under this proposal for a duration of next 3 months.

Authorized by	Name	Signature	Date
Chairman:	Dr. T D Babu		14.10.2020
Member Secretary:	Dr. Achuthan C R		14.10.2020
Main Nominee of CPCSEA:	Dr. C B Devanand		14.10.2020

(Kindly make sure that minutes of the meeting duly signed by all the participants are maintained by Office)

Publications and Conference Presentations

Journal papers

- [1] **Aiswariya, K.S.**, Jose, V. Photo-Mediated Facile Synthesis of Silver Nanoparticles Using *Curcuma zanthorrhiza* Rhizome Extract and Their In Vitro Antimicrobial and Anticancer Activity. *J Inorg Organomet Polym* 31, 3111–3124 (2021). <https://doi.org/10.1007/s10904-021-01951-0>
- [2] **Aiswariya, K.S.**, Jose, V. Bioactive Molecules Coated Silver Oxide Nanoparticle Synthesis from *Curcuma zanthorrhiza* and HR-LCMS Monitored Validation of Its Photocatalytic Potency Towards Malachite Green Degradation. *J Clust Sci* (2021). <https://doi.org/10.1007/s10876-021-02099-0>
- [3] Jose V, Raphel L, **Aiswariya K S**, Mathew P. Green synthesis of silver nanoparticles using *Annona squamosa* L. seed extract: characterization, photocatalytic and biological activity assay. *Bioprocess Biosyst Eng*. 2021 Apr 6. [doi: 10.1007/s00449-021-02562-2](https://doi.org/10.1007/s00449-021-02562-2). Epub ahead of print. PMID: 33822248.

Conference presentations

- [1] **Aiswariya K S**, Vimala Jose., ‘Degradation of malachite green using green synthesized AgNPs as photocatalysts’ at the International Conference on Water (ICW 2018) held at Kottayam and was selected as one among the best 10 posters.
- [2] **Aiswariya K S**, Vimala Jose., ‘Photocatalytic and Antimicrobial activity of aqueous extract mediated green synthesis of silver oxide nanoparticles’ in the two days International Conference on Nanomedicine (ICON -2019), held at Madurai Kamaraj University, Madurai, Tamil Nadu.
- [3] **Aiswariya K S**, Vimala Jose., ‘Antibacterial and Haemolytic activity of Green Synthesised Silver oxide nanoparticles using plant rhizome extract’ in the

National Seminar on Emerging Trends in Genomic Research, at St. Thomas' College (Autonomous), Thrissur, Kerala.

[4] **Aiswariya K S**, Vimala Jose., 'Effect of Phytosynthesised silver oxide nanoparticles on the degradation of an anionic dye – Coomassie Brilliant Blue' in the 31st Kerala Science Congress, held at Fatima Mata National College, Kollam.

[5] **Aiswariya K S**, Vimala Jose., 'Phytosynthesised silver nanoparticles assisted catalytic degradation of dyes' in National Seminar on New Frontiers in Material and Environmental Sciences (NFMES – 2020) held at S H Thevara, Ernakulam, Kerala.



Photo-Mediated Facile Synthesis of Silver Nanoparticles Using *Curcuma zanthorrhiza* Rhizome Extract and Their In Vitro Antimicrobial and Anticancer Activity

K. S. Aiswariya¹ · Vimala Jose¹

Received: 10 December 2020 / Accepted: 15 February 2021

© The Author(s), under exclusive licence to Springer Science+Business Media, LLC part of Springer Nature 2021

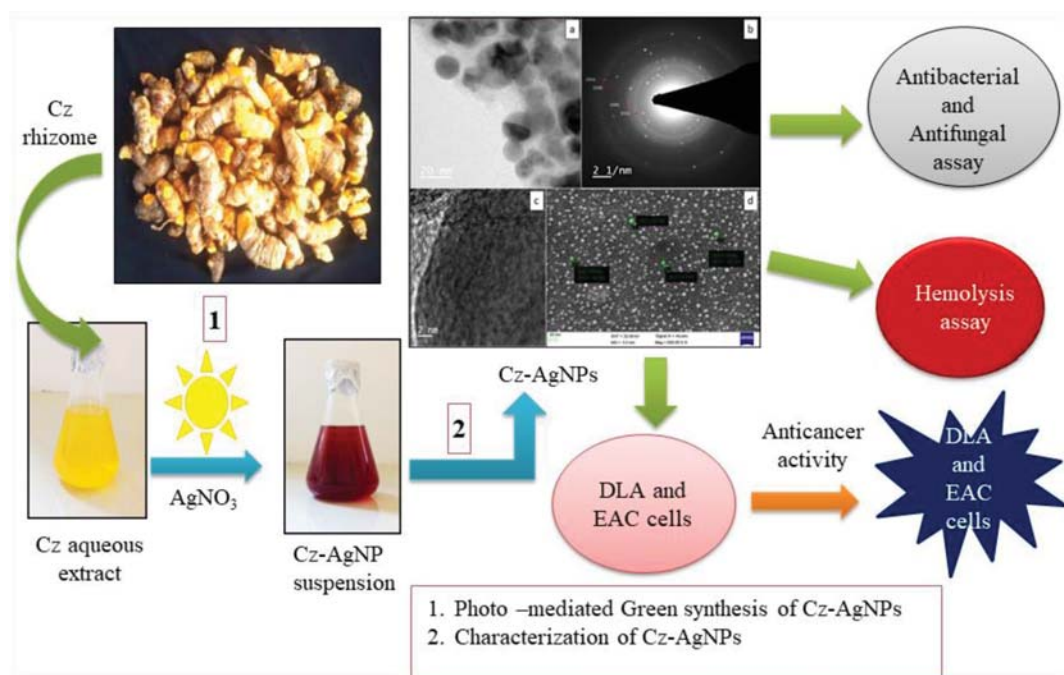
Abstract

Plants possess unique bioactive principles justifying their multifunctional properties. In this work silver nanoparticles (AgNPs) were prepared via a photo-mediated green approach for enhanced antimicrobial and anticancer activity. The aqueous rhizome extract of *Curcuma zanthorrhiza* Roxb. (Cz) was employed as a source of reducing and capping agent for the synthesis of colloidal Cz-AgNPs. The materialization of Cz-AgNPs was identified from the surface plasmon resonance observed at 416 nm using UV–Visible spectrophotometer. The FTIR analysis of both Cz-AgNPs and plant rhizome extract revealed the as-synthesized Cz-AgNPs were capped with plant derived phytoconstituents. The crystallinity, surface morphology, hydrodynamic size and surface area of Cz-AgNPs were characterized by PXRD, HR-TEM, FESEM, DLS and BET analysis. The as-synthesized Cz-AgNPs exhibited strong antimicrobial activities against bacterial strains and plant pathogenic fungi in a dose-dependent manner. The antimicrobial activity of Cz-AgNPs was assessed using standard disc diffusion, broth microdilution assay for bacterial strains and poisoned food technique for fungal strains. The Cz-AgNPs were inhibitory to all the microbes even at the lowest concentration. The biocompatible nature of Cz-AgNPs was analyzed for hemolytic properties with human erythrocytes and promising results were observed. In addition, the cytotoxicity activity (Trypan Blue Exclusion Method) on the cell lines of Dalton's Lymphoma Ascites (DLA) and Ehrlich Ascites Carcinoma (EAC) showed Cz-AgNPs exhibited potential anticancer activity with concentration as low as 1.67 µg/mL and 1.84 µg/mL respectively (IC₅₀ value). This work attempted at optimizing a safe dosage of silver nanoparticles using hemolysis assay and thus for application in therapy.

✉ Vimala Jose
vimalajoseparaemackel@gmail.com

¹ Centre for Bionanotechnology, Research and Post Graduate
Department of Botany, St. Thomas' College, University
of Calicut, Thrissur, Kerala 680001, India

Graphic Abstract



Keywords Aqueous rhizome extract · Face centered cubic structure · MIC · Hemolysis · Cytotoxicity

1 Introduction

Nanoparticles (NPs) have revolutionized the fields of materials science and medicine. They are exploited in the realms of catalysis [1], sensor technology [2], site specific drug delivery [3], imaging and cancer treatments [4]. Unfortunately, the majority of physicochemical techniques employed for the synthesis of metallic nanoparticles require the use of toxic solvents. The by-products from these processes pose a serious threat to the environment [5]. Therefore, in recent times, synthesis of metal nanoparticles using natural materials such as microbes, parasites, yeast, seaweeds and plants [6] has gained considerable interest among researchers.

Natural products derived from plants have contributed enormously in the treatment of ailments. The natural products obtained from plants possess bioactive principles. They are unique to each plant which justifies their role in therapeutics as analgesic, anticancer, anti-inflammatory, antihyperglycemic and lipolytic agents. Hence, they continue to be a critical source of contemporary drugs [7]. Phytoconstituents have the potential to interact with various other compounds through a variety of chemical reactions [8]. Apart from the medicinal properties, the chelating and antibacterial capabilities of different plants and

phytoplanktons are used to treat wastewater [9]. In addition, the tanning activity of plant polyphenols have been exploited in the leather industry [8]. On the other hand, their potency is inhibited due to their low hydrophilicity and stability. The natural products are mostly regarded as vulnerable drug candidates because of their requirements in high dosages and repeated administrations [10]. Despite the advantages of the biomolecules, the exploitation of the plant resources remains in a nascent stage.

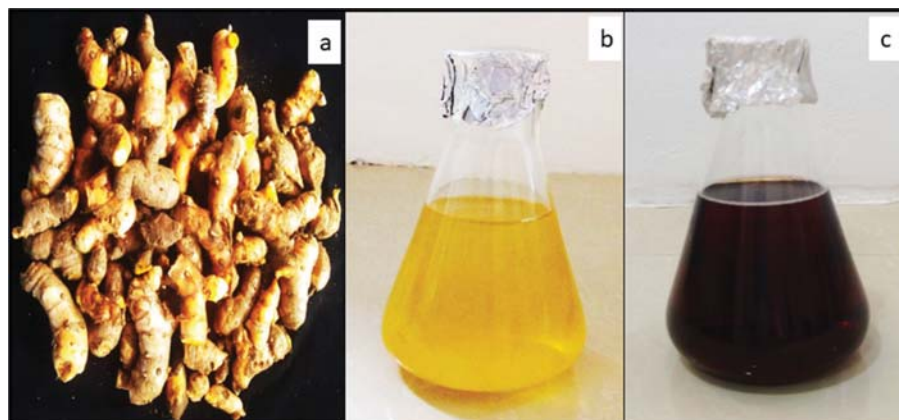
Consequently, during the recent years, synthesis of plant-based functional nanoparticles has emerged as an area of investigation among the scientific community [11]. Besides, the minimal efforts involved in synthesis, the plant material integrated nanoparticles show biocompatibility and biodegradability [12]. Therefore, the green synthesized nanoparticles have been explored in the field of nanomedicine as well. They are used in bioimaging [13], cancer theranostics [12, 14], as anti-cancerous agents [15], antibacterial [6, 16], antifungal [17], antiviral, anti-inflammatory, [14], antidiabetic [18], antioxidant [19] agents and also in wound dressing [20]. In this context, synthesis and utilization of Ag and AgNP-based materials has gained interest due to its morphology, biophysical properties and stability [21]. The green synthesized silver nanoparticles

also find its application in the degradation of pesticides [22], toxic dyes [23], as environmental sensors [24], in heavy metal removal [25–27] and mosquito control [28].

However, the properties of the green synthesized nanoparticles not only depend on the phytoconstituents present in the plant but also the reaction conditions employed during the synthesis. The synthesis of metallic nanoparticles utilizing plant's concentrates has been accounted for different plants, such as *Rheum palmatum* [29], *Ficus hispida* [30], *Cinnamomum verum* [23], *Combretum erythrophyllum* [31], *Morus indica* [32], *Eriobotrya japonica* [33], *Zingiber officinale* [34], *Sesbania grandiflora* [35], *Taraxacum officinale* [36], *Aspilia pluriseta* [37], *Caesalpinia pulcherrima* [38], *Sansevieria roxburghiana* [39]. But there is still a wide spectrum of plant metabolites which are yet to be investigated. For instance, the rhizomes of *Curcuma zanthorrhiza* Roxb. (Cz) which are rich in phenols, alkaloids, flavonoids, tannins, curcuminoids, terpenoids and xanthorhizol [40], have not been exploited so far in the synthesis of AgNPs. The presence of these secondary metabolites accounts for its medicinal properties such as diuretic, anticancer, antioxidant, antibacterial, antifungal, anti-inflammatory and hepatoprotective effects [41, 42]. Besides, *C. zanthorrhiza* is used as a cosmetic herb in South Asia [43].

Based on the above considerations, an attempt has been made in this paper to synthesize silver nanoparticles for the first time using the aqueous rhizome extract of *C. zanthorrhiza* Roxb. Further, to characterize the as-synthesized nanoparticles using different spectroscopic and electron microscopic techniques. The in vitro antibacterial, antifungal, hemolytic and cytotoxic potential of the as-synthesized silver nanoparticles (Cz-AgNPs) has also been investigated. The novelty of the present work lies in the usage of rhizome extracts of *C. zanthorrhiza*, which is a cheap, renewable and easily available resource. The results suggest the utilization of Cz-AgNPs as a promising chemotherapeutic drug.

Fig. 1 **a** Fresh rhizomes of *C. zanthorrhiza*, **b** 10% aqueous rhizome extract of *C. zanthorrhiza* (Yellow colour), **c** Cz-AgNPs suspension formed after the addition of 1 mM AgNO_3 solution to the plant rhizome extract (Reddish brown colour), exposed to sunlight for 1 h (Color figure online)



2 Materials and Methods

2.1 Preparation of Rhizome Extract

Curcuma zanthorrhiza rhizomes (Fig. 1a) were collected from the germplasm of Regional station of National Bureau of Plant Genetic Resources (NBPGR), Thrissur, Kerala, India. Rhizomes were washed with distilled water, dried in shade, and ground into fine powder. Subsequently, 10% (w/v) aqueous rhizome extract was prepared by boiling 10 g rhizome powder in 100 mL deionized water for 30 min. Thereafter, the aqueous rhizome extract was filtered using Whatman no.1 filter paper and the filtrate was centrifuged at 5000 rpm. The supernatant thus obtained was stored at 4 °C for subsequent experiments.

2.2 Green Synthesis of Silver Nanoparticles (Cz-AgNPs)

The aqueous solution of *C. zanthorrhiza* rhizome extract was taken in Erlenmeyer flask and 1 mM silver nitrate (Sigma Aldrich) solution was added to it (in the ratio 1:10 by volume). The flask was kept under stirring in sunlight for 1 h. After an hour of stirring, silver nanoparticles (Cz-AgNPs) were obtained. The nanoparticles were separated from the solution by repeated centrifugation at 12,000 rpm (Eppendorf 5430R). Finally, they were washed with deionized water to remove the water soluble biomolecules and the nanoparticle suspension was lyophilized. The lyophilized nanoparticle suspension was used for all the further experiments.

2.3 Characterization of Cz-AgNPs

The formation of Cz-AgNPs using the aqueous plant rhizome extract as reducing agent was monitored by recording the UV-Visible spectra of the solution using UV-Visible spectrophotometer (Shimadzu UV probe 1800), at a

resolution of 1 nm in the scanning range 600–300 nm. The infra-red spectra of both the plant rhizome extract and Cz-AgNPs were analyzed to understand the specific functional groups in the phytochemicals which are responsible for the reduction and stabilization of nanoparticles. The Fourier Transform Infra-Red (FTIR) spectra were recorded using Thermo Nicolet, Avatar 370 FTIR spectrophotometer in the spectral range of 4000–500 cm^{-1} and resolution of 4 cm^{-1} . Powder X-ray diffraction (XRD) pattern of the Cz-AgNPs was collected on a Malvern Panalytical Aeris diffractometer using Ni-filtered CuK α radiation. The data was collected with a step size of 0.02° and count time of 2 s per step over the range $10^\circ < 2\theta < 80^\circ$. The average crystallite size of Cz-AgNPs was calculated using the Scherrer equation, where, $D = k\lambda/\beta_{1/2} \cos \theta$ where, D = average crystallite size, k = Scherrer's constant (0.94), λ = X-ray wavelength, $\beta_{1/2}$ = pure diffraction broadening peak at half height and θ = diffraction angle. High-Resolution Transmission Electron Microscope (HR—TEM, Tecnai G2, F30) operated at 300 kV was used to examine the size, diffraction ring pattern (SAED), lattice fringes and d spacing of the as-synthesized silver nanoparticles. Further, the topography of the Cz-AgNPs was observed using Karl Zeiss FESEM Supra 55 Field Emission Scanning Electron Microscope (FESEM) operated at an accelerating voltage of 20 kV. The hydrodynamic particle size of the Cz-AgNPs was measured using Dynamic Light Scattering (DLS) technique (Horiba Scientific SZ-100). The measurement parameters included 633 nm wavelength, scattering angle of 90°, temperature of 25 °C, and dispersion medium viscosity of 0.894 mPa s. The specific area of the Cz-AgNPs was determined using the surface area and porosity analyzer (BET), Belsorp Mini 11, BEL Japan. The porosity was measured using a nitrogen adsorbent isotherm at 77 °C. Total pore volume and pore size were estimated by BJH method.

2.4 Antibacterial Activity of Cz-AgNPs

2.4.1 Disc Diffusion Method

Antibacterial activity of silver nanoparticles was analyzed using Kirby—Bauer disc-diffusion method [44] against selected bacterial strains, *Staphylococcus aureus* (MTCC96) and *Escherichia coli* (MTCC40). The pure cultures obtained from Institute of Microbial Technology, Chandigarh, India were used for the experiment. Initially, a prepared nutrient agar (Sigma-Aldrich, 28 g/L) was poured on sterile petriplates and allowed to solidify. Agar surface of each plate was then smeared with a sterile cotton swab of the selected bacterial strain. Subsequently, the sterile discs impregnated with 20 μL of various concentrations (10, 25, 50, 75, and 100 $\mu\text{g}/\text{mL}$) of Cz-AgNPs were allowed to dry in sterile conditions. Later it was placed on solidified agar plates at equal distance

along with control. Vancomycin disc (Sigma-Aldrich) was used as the positive control and a disc with deionised water served as the negative control. In addition, discs with 20 μL of 1 mM silver nitrate solution and 0.1 g/mL plant rhizome extract were also maintained. The plates (in triplicate) were then incubated at 37 °C, and the zone of inhibition (ZOI) was measured in mm after 24 h.

2.4.2 Broth Microdilution Assay

Six serial dilutions (10^{-1} , 10^{-2} , 10^{-3} , 10^{-4} , 10^{-5} , 10^{-6} mL) of clinical isolates of *E. coli* and *S. aureus* were made using the Luria Bertani (LB) broth (Sigma-Aldrich). Thereafter 1 mL each of bacterial suspension from 10^{-5} dilution was transferred to the sterile petriplates and molten nutrient agar was added to it. The petriplates were incubated overnight, after thorough rotation. Subsequently, 4 to 5 colonies from the nutrient agar plate were inoculated into the LB broth. The culture was read at 600 nm to adjust the final inoculum to 5×10^5 cfu/mL.

For the broth microdilution test, 50 μL of each bacterial suspension (*E. coli*, *S. aureus*) in LB broth was added to the wells of a sterile 96-well microtitre plate which already contained 50 μL of two-fold serially diluted antibiotic (Ampicillin), Cz-AgNPs, plant rhizome extract and silver nitrate solution in LB broth medium respectively. The highest concentration of antibiotic and Cz-AgNPs was 10 mg/L. 10 mg/L solution was further diluted to 512, 256, 128, 64, 32, 16, 8, 4, 2 and 1 $\mu\text{g}/\text{mL}$ and the end volume in each well was maintained at 100 μL . The wells 11 and 12 served as the growth control and sterile control, respectively. The contents of each well were mixed up and down using micropipettes before incubation for 24 h. The MIC (Minimum Inhibitory Concentration) was the lowest concentration of inoculum where no growth was observed after 24 h incubation with test solutions [45]. The respiratory activity was determined by adding 10 $\mu\text{L}/\text{well}$ of TTC (2,3,5- triphenyl tetrazolium chloride, Sigma-Aldrich) dissolved in water (TTC 20 mg/mL) and incubated for 30 min in the dark [46]. The plates were read with a microplate reader (BIO-Base) at 600 nm. The wells with bacterial suspension in an appropriate growth medium served as positive control. The wells with growth medium containing plant rhizome extract served as negative control. All measurements of MIC values were repeated in triplicates.

2.5 Antifungal Activity of Cz-AgNPs

For evaluating the antifungal activity of Cz-AgNPs, poisoned food technique [47] was followed. The Potato Dextrose Agar (PDA) was prepared (HiMedia—39 g/L) and kept in molten state at 70–80 °C. One third of the petriplates were filled with this molten agar. The various concentrations of

Cz-AgNP solution (10, 25, 50, 75 and 100 µg/mL) were prepared. 2 mL of CzAgNP solution was pipetted into each plate, mixed well and allowed to solidify. A PDA plate with 2 mL each of sterile distilled water and fluconazole (100 µg/mL) served as negative and positive control respectively. Additionally, PDA plates with 2 mL of 1 mM silver nitrate solution and plant rhizome extract (0.1 g/mL) were also maintained. Inoculum discs were cut with a potato borer (4 mm diameter) from a pure culture plate of *Aspergillus niger*, obtained from Pathology division, Kerala Agricultural University, Thrissur, Kerala, India. The plug of *A. niger* with the mycelial surface facing downwards was inoculated in the centre of each agar plate. The plates were incubated at 37 °C in dark condition for 7 days and the colony diameter was measured in mm. Three replicates were maintained. The fungi toxicity of the Cz-AgNP solution in terms of percentage of inhibition of mycelial growth was calculated using the formula.

$$\text{Percentage of inhibition} = C - T/C \times 100$$

where, C = Average increase in mycelial growth in the control plate (negative control). T = Average increase in the mycelial growth in the treatment plate.

2.6 Hemolysis Assay of Cz-AgNPs

Hemolysis experiments have been performed according to the method of Lin and Haynes, 2010 [48]. The fresh human

$$\text{Percentage of cytotoxicity} = \frac{\text{No. of dead cells}}{\text{No. of live cells} + \text{No. of dead cells}} \times 100.$$

blood samples used for the experiments were collected from (healthy, non-smoker) volunteers. Initially, 2 mL of the whole blood sample was added to 4 mL phosphate-buffered saline (PBS), centrifuged at 7800 rpm for 5 min at 4 °C to isolate red blood cells (RBCs). The isolated RBCs were further washed, re-suspended in 10 mL PBS and finally diluted to 20 mL with PBS. RBC suspension of 0.4 mL was exposed to 1.6 mL of varied concentrations (2, 10, 50, 100, 200 µg/mL) of Cz-AgNPs suspension in PBS (test group), 1 mM silver nitrate solution (test group), 1% saline Triton X-100 (positive control), and PBS (negative control). The samples were incubated at 37 °C. After 2, 4 and 6 h, the samples were centrifuged at 1600 rpm for 5 min and absorbance of the supernatant was read at 577 nm. The hemolytic degree was calculated using the following formula:

$$\text{Hemolysis percentage} = \frac{(\text{Absorbance}_{(\text{test})} - \text{Absorbance}_{(\text{negative control})})}{(\text{Absorbance}_{(\text{positive control})} - \text{Absorbance}_{(\text{negative control})})} \times 100\%$$

2.7 In Vitro Cytotoxicity Assay of Cz-AgNPs

The Dalton's Lymphoma Ascites (DLA) and Ehrlich Ascites Carcinoma (EAC) cell lines collected from the peritoneal cavity of mice were washed with Phosphate Buffer Saline (PBS). It was centrifuged at 1500 rpm for 3 min to remove the traces of blood. The DLA and EAC cell pellets were re-suspended in PBS to get a concentration of 1×10^7 cells/mL and used for cytotoxicity analysis. Trypan Blue Exclusion method was performed to evaluate the in vitro cytotoxicity assay. Approximately 1×10^6 DLA cells were distributed into test tubes containing different concentrations of Cz-AgNPs (0.2, 0.6, 0.8, 1, 1.6 and 2.5 µg/mL), plant rhizome extract (10, 25, 55, 75, 100 µg/mL) and silver nitrate solution (0.2, 0.4, 0.5, 0.6, 0.8, 1 µg/mL) in 1 mL PBS. Various concentrations of Cz-AgNPs (1, 1.6, 1.8, 2, 2.5 and 3 µg/mL), plant rhizome extract (10, 25, 55, 75, 100 µg/mL) and silver nitrate solution (0.2, 0.4, 0.5, 0.6, 0.8, 1 µg/mL) were added to test tubes with 1×10^6 EAC cells and were made upto 1 mL with PBS. The test tubes with cancer cell lines and various drugs were incubated for 3 h at 37 °C. After the incubation period, 100 µL of 1% trypan blue was added to the test tubes and allowed to stand for 2 min. The live (unstained) and dead (stained) cells were counted using haemocytometer to determine the percentage of toxicity and the IC₅₀ values. The percentage of toxicity was calculated using the formula,

2.8 Statistical Analysis

The experimental data is expressed as mean ± standard deviation (n=3) for each sample using SPSS (version 21) software. The graphs were plotted using Sigma Plot 12.3 software.

3 Results and Discussions

3.1 Green Synthesis of Cz-AgNPs

Upon addition of rhizome extract of *C. zanthorrhiza* to 1 mM silver nitrate solution, an immediate change in the color of the solution was observed. A color change from yellow to light brown and to dark brown was observed as the reaction progressed under sunlight for 1 h (Fig. 1b, c).

The color change indicated the formation of silver nanoparticles at pH=5.65. The change in color could be attributed to the excitation of surface vibration plasmon in the silver nanoparticles [49]. A preview of literature suggested that the formation of nanoparticles often depends upon the reaction conditions. In general, the formation of silver nanoparticles required thermal decomposition and incubation of the reaction mixtures at room temperature for 180 min and 15 h respectively [50, 51]. However, in the present study, the formation of AgNPs was observed in 60 min indicating the significance of the plant rhizome extract in the facile and rapid synthesis of Cz-AgNPs.

3.2 Characterization of Cz-AgNPs

3.2.1 UV-Visible Spectroscopy

The formation of silver nanoparticles was analyzed by UV-Visible spectroscopy. From the UV-Visible spectrum, the surface plasmon resonance (SPR) peak of the silver nanoparticles was observed at 416 nm (Fig. 2a) [52, 53]. The broadening of peak in the UV-Visible spectrum indicated the polydisperse nature of the silver nanoparticles in the aqueous suspension [54]. The dark brown color of the solution could be attributed to the SPR of the solution which is generated due to the interaction of electromagnetic field with free conduction electrons [55].

3.2.2 Fourier Transform Infrared (FTIR) Spectroscopy

FTIR analysis was performed to identify the various functional groups of plant extract attached to the silver

nanoparticles which were responsible for the synthesis and stabilization of the nanoparticles. The FTIR spectra of both the plant rhizome extract and the Cz-AgNPs are displayed in Fig. 2b. The IR spectrum of the plant rhizome extract showed absorption bands at 3467.55 cm^{-1} , 2075.13 cm^{-1} , 1643.13 cm^{-1} , 1074.20 cm^{-1} and 557.25 cm^{-1} . These bands could be assigned to phenolic OH group, C=O stretching vibrations, NH bond of amine group, CO stretching, and CH bending of alkynes respectively [31, 56, 57]. The characteristic absorption bands of Cz-AgNPs were observed at 3448.27 cm^{-1} , 2057.78 cm^{-1} , 1637.35 cm^{-1} , 1049.14 cm^{-1} and 541.92 cm^{-1} . The large shift observed in the absorption bands of the Cz-AgNPs indicated the capping of phytoconstituents in the plant rhizome extract onto the as-synthesized silver nanoparticles. The capping of active molecules on the nanoparticles masks the extreme toxicity found in synthetic nanoparticles. It also enhances the synergistic activity of plant derived secondary metabolites and nanoparticles. The stability of the silver nanoparticles in aqueous medium was probably due to the amide linkage of proteins with Cz-AgNPs [58].

3.2.3 X-Ray Diffraction (XRD) Analysis

The XRD pattern of Cz-AgNPs is depicted in Fig. 3. The well-defined characteristic Bragg's reflection peaks of face centred cubic structure of the metallic silver were observed at 2θ values 38.14° , 46.19° , 64.53° and 77.44° corresponding to the Miller Indices of (111), (200), (222) and (311) planes respectively [59]. The obtained results were found to be in good agreement with JCPDS No. 00-004-0783 indicating the formation of face centred

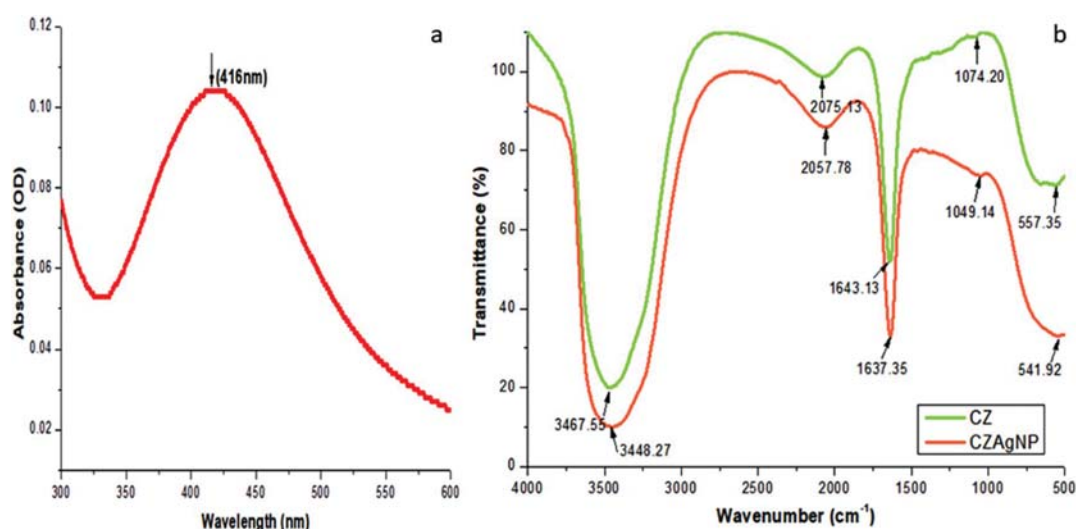


Fig. 2 a UV-Visible absorption spectra of Cz-AgNPs with $\lambda_{\text{max}}=416\text{ nm}$ at pH 5.65, b FTIR spectrum of the plant rhizome extract (Cz) and synthesized Cz-AgNPs

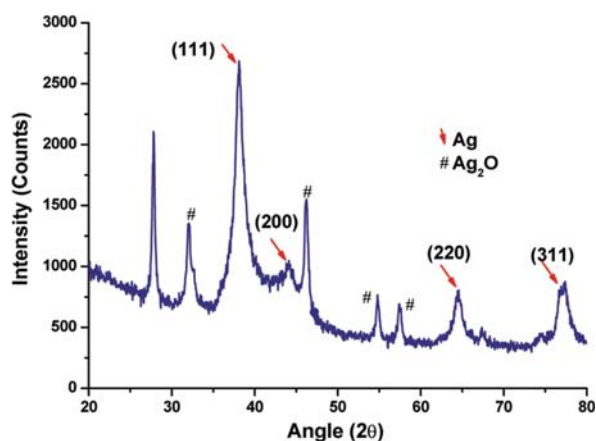


Fig. 3 PXRD pattern of Cz-AgNPs with well characterized Bragg's Reflection peaks at (111), (200), (220) and (311) planes attributing to fcc structure with average crystallite size 17.278 nm

cubic silver. In contrast to the other planes, the intense peak at (111) plane could specify the direction of growth of the synthesized silver nanoparticles [30]. The crystallite size of the silver nanoparticles was determined using Scherrer equation and the average crystallite size of the Cz-AgNPs was found to be 17.278 nm. In addition, four weak peaks corresponding to the silver oxide nanoparticles were observed at 32.23°, 46.10°, 54.57° and 57.39° (JCPDS No. 76-1393). Another peak at 27.82° could be correlated to the silver chloride nanoparticle (JCPDS No. 31-1238).

3.2.4 Electron Microscopy

The size and morphology of the as-synthesized nanoparticles were determined by HR-TEM and FESEM. The HR-TEM images revealed that the Cz-AgNPs were spherical and crystalline in nature. The d-spacing of 0.236 nm was observed

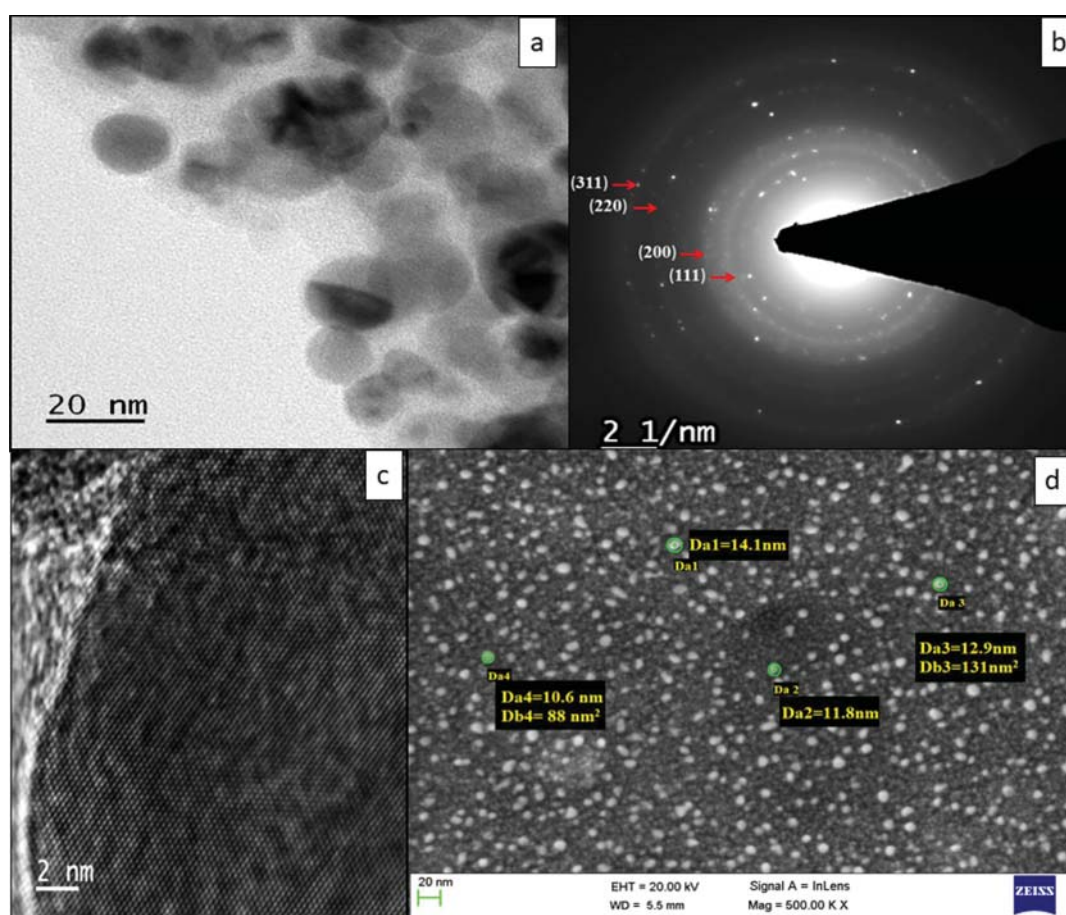
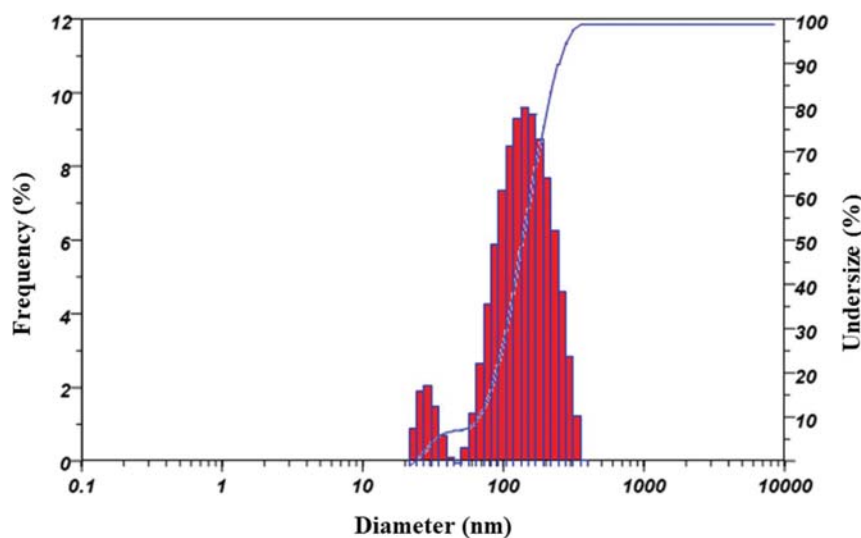


Fig. 4 **a** HR-TEM image revealing the spherical nature of Cz-AgNPs, **b** SAED pattern of Cz-AgNPs indicating polycrystalline nature with planes coherent to PXRD pattern, **c** HR-TEM image with lattice

fringes (d- spacing), **d** FESEM micrograph depicting the spherical morphology of Cz-AgNPs

Fig. 5 Hydrodynamic particle size distribution of Cz-AgNPs measured by DLS analysis



for (111) orientation. The value was in good agreement with that reported for free silver centers ($d_{111} = 0.2359$ nm) (Fig. 4a). The value is hardly distinguishable from Soman and Ray [59] who have obtained a d-spacing value of 0.235 nm for the silver nanoparticles synthesized in this regard. Further the polycrystalline nature of the Cz-AgNPs was revealed from the bright circular spots in the SAED pattern indicating the (111), (200) and (220) planes which were consistent with the obtained XRD pattern (Fig. 4b, c). Moreover, the FESEM micrographs also revealed the spherical morphology of the as-synthesized Cz-AgNPs (Fig. 4d). The average particle size of the Cz-AgNPs was found to be ranging from 10.6 to 15.31 nm.

3.2.5 Dynamic Light Scattering (DLS) Analysis

The DLS results obtained for Cz-AgNPs are shown in Fig. 5. It is observed that the size distribution of Cz-AgNPs ranges from 20 to 145 nm with a Z-average of 111.2 nm and a polydispersity index of 0.348. The size of the Cz-AgNPs obtained from DLS is larger compared to the electron microscopic analysis. The difference in the size of the as-synthesized nanoparticles is due to the influence of Brownian motion [60]. Moreover, this disparity in size could be possibly due to the capping of plant metabolites and adsorption of water on to the as-synthesized silver nanoparticles [33].

3.2.6 BET Surface Analysis

The Nitrogen adsorption–desorption isotherm of Cz-AgNPs were measured using volumetric gas adsorption analyzer. The Nitrogen sorption isotherm of Cz-AgNPs is depicted in Fig. 6. It shows the as-synthesized nanoparticle presents typical IV adsorption. It can be seen from the

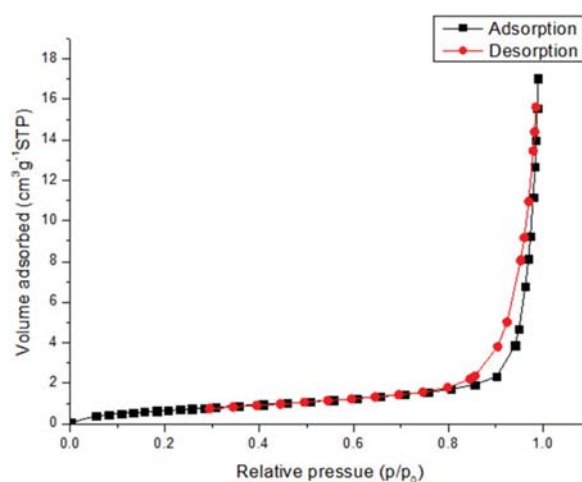


Fig. 6 Nitrogen adsorption–desorption isotherms of Cz-AgNPs

figure, at relative low pressure, the isotherm are flat, which describes the adsorption of Cz-AgNPs mostly occurs in the mesopores. The rapid increase in isotherms and formation of lag loop at relatively high pressure is due to capillary agglomeration phenomenon [61].

From the multipoint BET equation, the calculated specific surface area of Cz-AgNP is 2.683 m²/g and monolayer adsorption volume is 0.614 cm³/g (Fig. 7). The cumulative pore volume and pore diameter from the BJH size distribution were found to be 2.634 cm³ and 39.213 nm respectively. The results ascertained that the as-synthesized nanoparticles are porous with mesoporous nature.

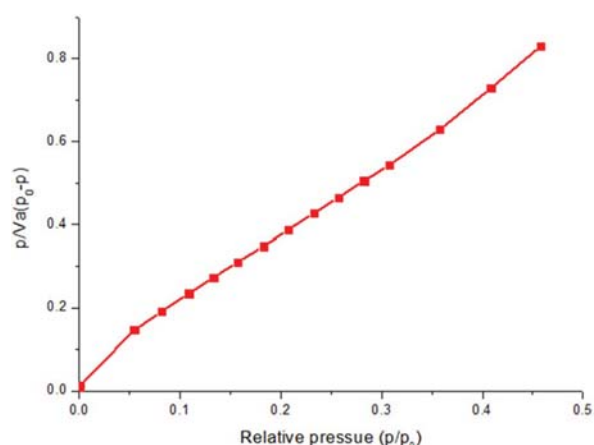


Fig. 7 BET plots of as-synthesized silver nanoparticles at 77 °C

Table 1 Zone of inhibition of various test solutions against bacterial strains (disc diffusion method)

Drug (concentration)	Zone of inhibition (mm)	
	<i>E. coli</i>	<i>S. aureus</i>
Vancomycin (30 mcg)	9.5 ± 0.5	14.9 ± 0.1
Distilled water (control)	Nil	Nil
Cz-AgNPs (100 µg/mL)	8.95 ± 0.05	7.00 ± 0.1
Cz-AgNPs (75 µg/mL)	7.96 ± 0.05	3.9 ± 0.1
Cz-AgNPs (50 µg/mL)	8.00 ± 0	3.83 ± 0.12
Cz-AgNPs (25 µg/mL)	5.93 ± 0.05	3.03 ± 0.15
Cz-AgNPs (10 µg/mL)	4.90 ± 0.1	2.10 ± 0.1
AgNO ₃ solution (1 mM)	2.00 ± 0.1	1.33 ± 0.15
Plant rhizome extract (0.1 g/mL)	Nil	1.00 ± 0.10

Values are expressed as Mean ± SD; n = 3

3.3 Antimicrobial Activity of Cz-AgNPs

3.3.1 Disc Diffusion Method

In disc diffusion assay, the as-synthesized Cz-AgNPs displayed an efficient inhibitory activity against *E. coli* and *S. aureus*. The highest ZOI at 100 µg/mL concentration of Cz-AgNPs was 8.95 ± 0.05 mm and 7 ± 0.1 mm respectively for *E. coli* and *S. aureus*. However, concentration in the range of 10 µg/mL to 75 µg/mL also showed slight inhibition in bacterial growth. The silver nitrate solution and plant rhizome extract alone exhibited negligible activity against the selected bacterial strains. The vancomycin disc exhibited 9.5 ± 0.5 mm and 14.9 ± 0.1 mm ZOI against *E. coli* and *S. aureus* respectively (Table 1).

3.3.2 Broth Microdilution Assay

The Broth microdilution assay explains the MIC of the as-synthesized Cz-AgNPs against two strains of bacteria. After 24 h of incubation, the wells with no color change were scored for the MIC value and the wells stained with dark red color showed the presence of bacteria. The MIC was found to be 4 µg/mL and 32 µg/mL respectively for ampicillin and Cz-AgNPs against *S. aureus*. In the case of *E. coli*, the MIC was 16 µg/mL and 64 µg/mL for the antibiotic ampicillin and Cz-AgNPs. The plant rhizome extract showed the least activity against both the bacterial strains in which the MIC was 512 µg/mL. The MIC of silver nitrate solution was 64 µg/mL for both the bacterial isolates (Fig. 8).

The possible mechanism of antibacterial activity can be attributed to the ultra-small size. And the increased surface to the volume ratio of the nanoparticles which can destroy the membrane, cross the body of the microbe. It can result in ROS generation and finally intracellular damage [62]. It has been observed that size, concentration and shape of the silver nanoparticle can affect its anti-microbial activity. It was found that *E. coli* responded best to triangular-shaped nanoparticles compared to spherical and rod-shaped ones as the triangular shape provides more positive charge to the nanoparticles, ensuring greater antibacterial activity [63]. Therefore, almost equal ZOI exhibited by the Cz-AgNPs and vancomycin for *E. coli* could be attributed to the spherical nature of the as-synthesized nanoparticles rather than triangular nature and also the less surface area of the nanoparticles which was ascertained from nitrogen physisorption. The decrease in ZOI exhibited by Cz-AgNPs in gram-positive bacteria *S. aureus* is perhaps due to the complexity in the composition of the cell wall, which hinders the anchoring of silver nanoparticles onto the bacterial cell wall, thereby obstructing the antibacterial activity [62]. Several researchers have reported the potential of biosynthesized AgNPs as efficient microbicides against various clinical isolates [15, 16]. Novel reports ascertain the resistance of certain bacterial strains to biosynthesized silver nanoparticles. A study by Aina et al. has reported that the efficacy of biosynthesized silver nanoparticles against *S. aureus* and *E. coli* was low even at a concentration 100 µg/mL [28]. This resistance in bacterial strains was due to the repeated exposure of silver nanoparticles buds from the production of flagellin. Flagellin is an adhesive protein, which triggers the agglomeration of nanoparticle, reduces their stability and thereby bring down the efficacy of silver nanoparticles as bactericides [64]. However, the results indicated that the Cz-AgNPs were relatively effective against *E. coli* than to *S. aureus*.

Fig. 8 MIC of Ampicillin (Ab), Cz-AgNPs, plant rhizome extract (PE) and AgNO₃ solution respectively against **a** *E. coli* and **b** *S. aureus*. (arrows represent MIC of respective drugs)

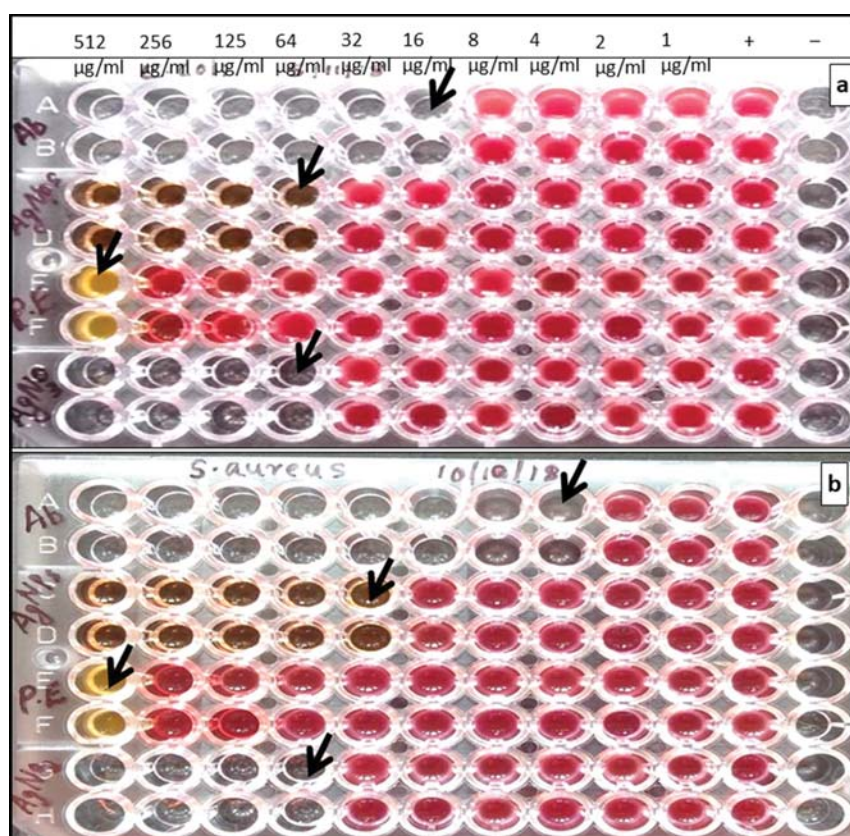


Table 2 Percentage of mycelial growth inhibition by various drugs against fungal pathogen *A. niger*

Drug (concentration)	Mycelial growth (mm)	Percentage of inhibition = $C - T/C \times 100$ (%)
Flucanazole (100 µg/mL)	16.50 ± 0.50	80.96
Distilled water (control)	86.66 ± 0.57	0
Cz-AgNPs (100 µg/mL)	11.83 ± 0.76	86.34
Cz-AgNPs (75 µg/mL)	30.00 ± 1.73	65.38
Cz-AgNPs (50 µg/mL)	34.00 ± 1.00	60.76
Cz-AgNPs (25 µg/mL)	35.66 ± 2.08	58.85
AgNO ₃ solution (1 mM)	47.66 ± 1.15	45.00
Plant rhizome extract (0.1 g/mL)	65.33 ± 3.78	24.61

Values are expressed as mean ± SD; n = 3

3.4 Antifungal Activity of Cz-AgNPs

The antifungal activity of various concentrations of Cz-AgNPs against *A. niger* is presented in Table 2. The rate of fungal growth inhibition was proportional to the concentration of Cz-AgNPs. The standard drug, fluconazole, inhibited 80.96% of fungal growth. The inhibition percentage of silver nitrate solution and plant rhizome extract against *A.*

niger was 45% and 24.61% respectively, whereas Cz-AgNPs showed 86.34% inhibition at a concentration of 100 µg/mL. Hence, the proliferation of *A. niger* was largely suppressed at a concentration of 100 µg/mL Cz-AgNPs, while the silver nitrate solution and the plant rhizome extract showed very low inhibition rate under the same concentration, demonstrating the antifungal activity of as-synthesized silver nanoparticles. The control group did not show any zone

Table 3 Hemolysis percentage of Cz-AgNPs and silver nitrate solution in the blood stream

Drug (concentration)	Percentage of hemolysis (%)		
	2 h Incubation	4 h Incubation	6 h Incubation
Cz-AgNPs			
2 µg/ml	0.02	0.09	0.15
10 µg/ml	0.06	0.20	0.39
50 µg/ml	0.10	0.24	0.52
100 µg/ml	0.12	0.38	0.81
200 µg/ml	0.20	0.52	1.22
AgNO ₃ solution (1 mM)	89	92	96

$$\text{Hemolysis percentage} = \frac{(\text{Absorbance}_{(\text{test})} - \text{Absorbance}_{(\text{negative control})})}{(\text{Absorbance}_{(\text{positive control})} - \text{Absorbance}_{(\text{negative control})})} \times 100\%$$

of inhibition. However, the antifungal activity of the metal nanoparticles depends on the size of the nanoparticles as well as on the type of fungus and the deformation of the fungal hyphae may be due to the membrane disintegrity [65]. Nevertheless, the as-synthesized silver nanoparticles have caused detrimental effects to the infectious filamentous fungi *A. niger* manifesting its efficacy in the development of potent antifungal agent. This might be due to the synergistic activity of the Cz-AgNPs formed by the capping of plant rhizome extract.

3.5 Hemolysis Assay of Cz-AgNPs

Nanomaterials should be biocompatible for them to be used for pharmaceutical purposes. One of the accepted methods to study biocompatibility is the hemolysis assay [66]. The biocompatibility of Cz-AgNPs was assessed in human RBCs

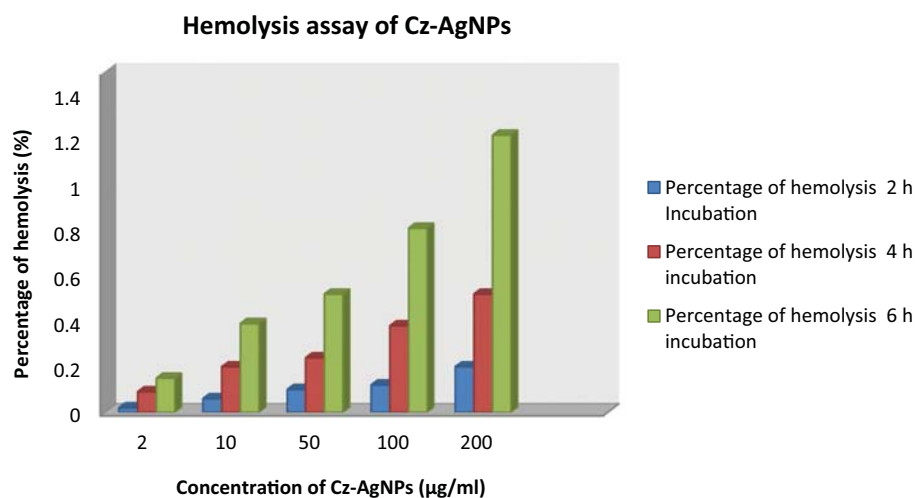
collected from healthy volunteers. The hemolytic activity was evaluated after 2 h, 4 h and 6 h of incubation. It was found that rate of hemolysis depends on concentration of test solution and the time of incubation (Table 3; Graph 1 and Fig. 9).

The results indicated that less than 1.5% hemolysis occurred in Cz-AgNPs treated groups even after 6 h of incubation, which was very close to PBS (negative control), whereas silver nitrate solution and Triton X (positive control) treated group exhibited 96% and 100% hemolysis respectively. According to ASTM E2524-08 standard, the acceptable blood damage criterion is below 5% [67]. Earlier research reports have shown that under optimal conditions green synthesized nanoparticles were biocompatible [58, 59]. The smallest sized silver nanoparticles displayed greater ability to induce membrane damage due to the direct interaction between RBC and nanoparticles. It results in stress and afterwards hemolysis [68]. Though, the present results stand well within the standard limits of biocompatibility, further studies are required before using the as-synthesized Cz-AgNPs for bioimaging and drug delivery.

3.6 In Vitro Cytotoxicity Assay of Cz-AgNPs

The short term in vitro cytotoxicity of Cz-AgNPs was compared with plant rhizome extract and silver nitrate solution using trypan blue exclusion method in DLA and EAC cell lines. The transparent viable cells and stained dead cells were counted using hemocytometer. The percentage cytotoxicity exhibited by the Cz-AgNPs, plant rhizome extract and silver nitrate solution on DLA and EAC cell lines are presented in Tables 4, 5. The plant rhizome extract, Cz-AgNPs and silver nitrate solution exhibited a dose-dependent cell death in both DLA and EAC cell lines. The IC₅₀ value of the plant rhizome extract,

Graph 1 Representation of hemolysis assay of green synthesized Cz-AgNPs



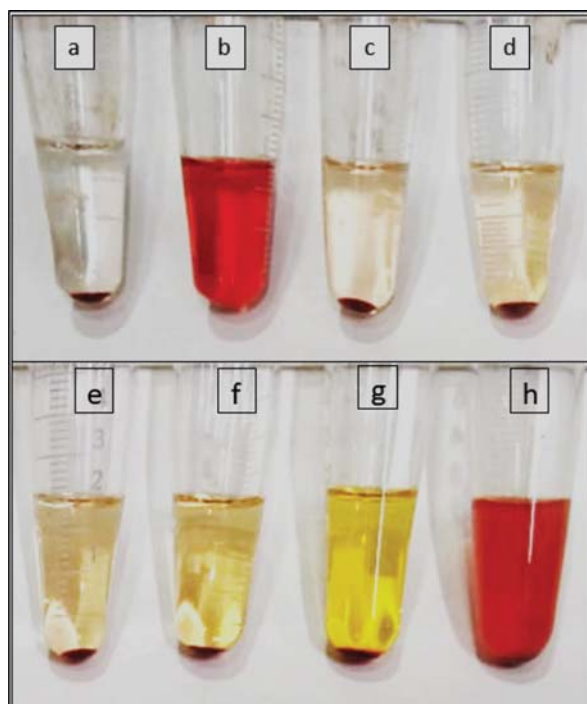


Fig. 9 Hemolysis activity **a** PBS, **b** Triton-X, **c** 2 $\mu\text{g/ml}$, **d–g** Cz-AgNPs at 10 $\mu\text{g/ml}$, 50 $\mu\text{g/ml}$, 100 $\mu\text{g/ml}$, 200 $\mu\text{g/ml}$ concentrations respectively and **h** AgNO_3 solution

Table 4 Comparison of percentage cytotoxicity of Cz-AgNPs, plant rhizome extract and silver nitrate solution against DLA cell lines

Drug	Concentration ($\mu\text{g/mL}$)	Percentage cytotoxicity (%)	IC ₅₀ value ($\mu\text{g/mL}$)
Cz-AgNPs	0.2	2.42	1.67
	0.6	6.95	
	0.8	13.65	
	1.0	18.74	
	1.6	34.17	
	2.5	93.75	
AgNO_3 solution	0.2	6.91	0.494
	0.4	13.34	
	0.5	53.94	
	0.6	76.74	
	0.8	83.2	
	1	95.68	
Plant rhizome extract	10	4.42	90.13
	25	7.62	
	35	19.41	
	55	21.15	
	75	42.35	
	100	62.5	

$$\text{Percentage of cytotoxicity} = \frac{\text{No. of dead cells}}{\text{No. of live cells} + \text{No. of dead cells}} \times 100$$

Table 5 Comparison of percentage cytotoxicity of Cz-AgNPs, plant rhizome extract and silver nitrate solution against EAC cell lines

Drug	Concentration ($\mu\text{g/mL}$)	Percentage cytotoxicity (%)	IC ₅₀ value ($\mu\text{g/mL}$)
Cz-AgNPs	1.0	14.39	1.84
	1.6	23.48	
	1.8	35.28	
	2.0	53.30	
	2.5	83.87	
	3.0	91.4	
AgNO_3 solution	0.2	7.66	0.513
	0.4	49.40	
	0.5	63.10	
	0.6	70.46	
	0.8	78.85	
	1	80.34	
Plant rhizome extract	10	17.17	50.23
	25	15.42	
	35	33.78	
	55	41.24	
	75	79.3	
	100	96.34	

$$\text{Percentage of cytotoxicity} = \frac{\text{No. of dead cells}}{\text{No. of live cells} + \text{No. of dead cells}} \times 100$$

Cz-AgNPs and silver nitrate solution in DLA cells was determined to be 90.13 $\mu\text{g/mL}$, 1.67 $\mu\text{g/mL}$ and 0.494 $\mu\text{g/mL}$ respectively. In EAC cell lines the IC₅₀ value was observed to be 50.23 $\mu\text{g/mL}$, 1.84 $\mu\text{g/mL}$ and 0.513 $\mu\text{g/mL}$ for the plant rhizome extract, Cz-AgNPs and silver nitrate solution respectively. It has been reported that 200 $\mu\text{g/mL}$ of silver nanoparticles synthesized using *F. hispida* leaf extracts, *Colpomenia sinuosa* and *Halymenia poryphyroides* completely inhibits DLA and EAC cells [55, 69]. Kanagamani et al. [70] reported that 50 $\mu\text{g/mL}$ of standard drug curcumin is required for 98.07% of inhibition of DLA cells. Interestingly, in our study 2.5 $\mu\text{g/mL}$ and 3 $\mu\text{g/mL}$ of silver nanoparticles synthesized using rhizome extract of *C. zanthorrhiza* inhibited 97.99% of DLA cells and 91.4% of EAC cells respectively. This finding validates that low doses of Cz-AgNPs can effectively inhibit the viability and proliferation of DLA and EAC cell lines.

The silver nanoparticles were found to inhibit the cell cycle by generating ROS resulting in the death of the cancer cells [71]. Many reports show that silver nanoparticles are effective against various cancer cell lines like MCF 7 (breast cancer) cells [72], Hep G2 cell lines of liver cancer [73]. However, in vivo experiments are to be performed before clinical trials and the development of new formulations of silver nanoparticles against tumor cell lines.

4 Conclusion

The green synthesis of AgNPs using *C. zanthorrhiza* aqueous rhizome extract has been reported the first time via photo-mediated process. The synthesis of Cz-AgNPs was confirmed using UV–Visible Spectroscopy with a Surface Plasmon Resonance band at 416 nm. PXRD pattern revealed the face centred cubic crystal structure of Cz-AgNPs with an average crystallite size of 17 nm. FTIR analysis demonstrated the efficient capping of plant derived phytoconstituents onto the Cz-AgNPs. HR-TEM and FESEM micrographs showed the spherical crystalline nature of Cz-AgNPs. The BET analysis revealed mesoporous nature of Cz-AgNPs. The results indicated that Cz-AgNPs can be used as antimicrobial agents against human pathogenic bacteria and plant pathogenic fungi. The present study also revealed the effects of as-synthesized Cz-AgNPs on anticancer activities by effectively inhibiting the viability and proliferation of DLA and EAC cell lines. The biocompatible nature of Cz-AgNPs was investigated by the hemolysis assay of human erythrocytes. The results are promising as they can contribute to the upgraded utilization of Cz-AgNPs for drug delivery and for therapeutic drug development.

Acknowledgements We gratefully acknowledge the Council of Scientific and Industrial Research for the fellowship, Amala Cancer Research Centre, Thrissur, Kerala, India for the cytotoxicity analysis, DST—FIST for the facilities at St. Thomas' College (Autonomous), Thrissur, SAIF at IIT Bombay for HR—TEM, Centre for Nanoscience and Nanotechnology, Sathyabama University for FESEM measurements and STIC Cochin University for FTIR analysis.

Compliance with Ethical Standards

Conflict of interest The authors have no conflicts of interest to declare that are relevant to the content of this article.

References

- N. Norouzi, M.K. Das, A.J. Richard, A.A. Ibrahim, H.M. El-Kaderi, S. El-Shall, *Nanoscale* **12**, 19191 (2020)
- P. Proposito, L. Burratti, I. Venditti, *Chemosensors* **8**, 1 (2020)
- M. Gisbert-Garzarán, J.C. Berkmann, D. Giasafaki, D. Lozano, K. Spyrou, M. Manzano, T. Steriotis, G.N. Duda, K. Schmidt-Bleek, G. Charalambopoulou, M. Vallet-Regí, A.C.S. *Appl. Mater. Interfaces* **12**, 14946 (2020)
- F. Ren, H. Liu, H. Zhang, Z. Jiang, B. Xia, C. Genevois, T. He, M. Allix, Q. Sun, Z. Li, M. Gao, *Nano Today* **34**, 100905 (2020)
- K.D. Lee, P.C. Nagajyothi, *J. Nanomater.* **2011**, 557 (2011)
- P.B. Dayma, A.V. Mangrola, S.P. Suriyaraj, P. Dudhagara, K. Rajesh, *J. Pharm. Chem. Biol. Sci.* **7**, 94 (2019)
- S.E. Cross, Y.S. Jin, Q.Y. Lu, J. Rao, J.K. Gimzewski, *Nanotechnology* **22**, 215101 (2011)
- S. Quideau, D. Defieux, C. Douat-Casassus, L. Pouységu, *Angew. Chem. - Int. Ed.* **50**, 586 (2011)
- O. OoKolawole, S. Oguntoye, O. Agbede, A. Olayemi, *Ethnobot. Leaflet* **10**, 228 (2006)
- A.R. Bilia, V. Piazzini, C. Guccione, L. Risaliti, M. Asprea, G. Capecci, M.C. Bergonzi, *Planta Med.* **83**, 366 (2017)
- C.L. Criado, *J. Nanomed. Res.* **2**, 2 (2015)
- M. Ovais, A.T. Khalil, A. Raza, M.A. Khan, I. Ahmad, N.U. Islam, M. Saravanan, M.F. Ubaid, M. Ali, Z.K. Shinwari, *Nanomedicine* **12**, 3157 (2016)
- R. Sankar, P.K.S.M. Rahman, K. Varunkumar, C. Anusha, A. Kalaiarasi, K.S. Shivashangari, V. Ravikumar, *J. Mol. Struct.* **1129**, 8 (2017)
- X.F. Zhang, Z.G. Liu, W. Shen, S. Gurunathan, *Int. J. Mol. Sci.* **17**, 1534 (2016)
- V. Castro-aceituno, V. Castro-aceituno, S. Ahn, S. Yesmin, P. Singh, *Biomed. Pharmacother.* **84**, 158 (2017)
- A.K.M.R. Uddin, M.A.B. Siddique, F. Rahman, A.K.M.A. Ullah, R. Khan, *J. Inorg. Organomet. Polym. Mater.* **30**, 3305 (2020)
- S. Ghojavand, M. Madani, J. Karimi, *J. Inorg. Organomet. Polym. Mater.* **30**, 2987 (2020)
- U.R. Shwetha, M.S. Latha, C.R. Rajith Kumar, M.S. Kiran, V.S. Betageri, *J. Inorg. Organomet. Polym. Mater.* (2020). <https://doi.org/10.1007/s10904-020-01575-w>
- M.S. Kiran, V.S. Betageri, C.R.R. Kumar, S.P. Vinay, M.S. Latha, *J. Inorg. Organomet. Polym. Mater.* **30**, 2916 (2020)
- G. Das, J.K. Patra, T. Debnath, A. Ansari, H.S. Shin, *PLoS ONE* **14**, 1 (2019)
- L.P. Silva, T.M. Pereira, C.C. Bonatto, *Frontiers and Perspectives in the Green Synthesis of Silver Nanoparticles* (Elsevier Inc., Amsterdam, 2019).
- N.A. Ramos-Delgado, L. Hinojosa-Reyes, I.L. Guzman-Mar, M.A. Gracia-Pinilla, A. Hernández-Ramírez, *Catal. Today* **209**, 35 (2013)
- U. Kamran, H.N. Bhatti, M. Iqbal, S. Jamil, M. Zahid, *J. Mol. Struct.* **1179**, 532 (2019)
- K.B.A. Ahmed, R. Senthilnathan, S. Megarajan, V. Anbazhagan, *J. Photochem. Photobiol. B* **151**, 39 (2015)
- S. Yari, S. Abbasizadeh, S.E. Mousavi, M.S. Moghaddam, A.Z. Moghaddam, *Process Saf. Environ. Prot.* **94**, 159 (2015)
- P. Nasehi, B. Mahmoudi, S.F. Abbaspour, M.S. Moghaddam, *RSC Adv.* **9**, 20087 (2019)
- P. Nasehi, M.S. Moghaddam, S.F. Abbaspour, N. Karachi, *Sep. Sci. Technol.* **55**, 1078 (2020)
- D.A. Aina, O. Owolo, A. Lateef, F.O. Aina, A.S. Hakeem, *Karbala Int. J. Mod. Sci.* **5**, 2 (2019)
- S. Arokiyaraj, S. Vincent, M. Saravanan, Y. Lee, Y.K. Oh, K.H. Kim, *Artif. Cells Nanomed Biotechnol.* **45**, 372 (2017)
- A.V. Ramesh, D.R. Devi, G.R. Battu, K. Basavaiah, S. Afr. J. Chem. Eng. **26**, 25 (2018)
- O.T. Jemilugba, E.H.M. Sakho, S. Parani, V. Mavumengwana, O.S. Oluwafemi, *Colloids Interface Sci. Commun.* **31**, 100191 (2019)
- S. Some, O. Bulut, K. Biswas, A. Kumar, A. Roy, I.K. Sen, A. Mandal, O.L. Franco, İ.A. İnce, K. Neog, S. Das, S. Pradhan, S. Dutta, D. Bhattacharjya, S. Saha, P.K. Das Mohapatra, A. Bhui-mali, B.G. Unni, A. Kati, A.K. Mandal, M.D. Yilmaz, I. Ocsoy, *Sci. Rep.* **9**, 1 (2019)
- B. Rao, R.C. Tang, *Adv. Nat. Sci. Nanosci. Nanotechnol.* **8**, 015014 (2017)
- A.R.M. Abd El-Aziz, M.R. Al-Othman, *Pak. J. Bot.* **51**, 443 (2019)
- M. Srinivasan, M. Venkatesan, V. Arumugam, G. Natesan, N. Saravanan, S. Murugesan, S. Ramachandran, R. Ayyasamy, A. Pugazhendhi, *Process Biochem.* **80**, 197 (2019)
- T. Rasheed, F. Nabeel, M. Bilal, H.M.N. Iqbal, *Biocatal. Agric. Biotechnol.* **19**, 101154 (2019)

37. A.O. Nyabola, P.G. Kareru, E.S. Madivoli, S.I. Wanakai, E.G. Maina, J. Inorg. Organomet. Polym. Mater. **30**, 3493 (2020)
38. P. Moteriya, S. Chanda, J. Inorg. Organomet. Polym. Mater. **30**, 3920 (2020)
39. A.G. Rama Krishna, C.S. Espenti, Y.V. Rami Reddy, A. Obbu, M.V. Satyanarayana, J. Inorg. Organomet. Polym. Mater. **30**, 4155 (2020)
40. H.P.A. Mary, G.K. Susheela, S. Jayasree, A.M. Nizzy, B. Rajagopal, S. Jeeva, Asian Pac. J. Trop. Biomed. **2**, S637 (2012)
41. C. Singgih Wahono, C. Diah Setyorini, H. Kalim, N. Nurdiana, K. Handono, Int. J. Rheumatol. (2017). <https://doi.org/10.1155/2017/7687053>
42. S. Anjusha, A. Gangaprasad, J. Pharmacogn. Phytochem. **3**, 50 (2014)
43. P.N. Ravindran, K. Nirmal Babu, K. Sivaraman, *Turmeric: The Genus Curcuma* (CRC Press, Boca Raton, 2007).
44. A.W. Bauer, W.M.M. Kirby, J.C. Sherris, A.M. Turck, A. Von Graevenitz, Am. J. Clin. Pathol. **45**, 493 (1978)
45. A. Mourey, N. Canillac, Food Control **13**, 289 (2002)
46. J.N. Eloff, Planta Med. **64**, 711 (1998)
47. Y.L. Nene, P.N. Thapliyal, *Fungicides in Plant Disease Control* (Oxford & IBH Publisher house, New Delhi, 1979).
48. Y.S. Lin, C.L. Haynes, J. Am. Chem. Soc. **132**, 4834 (2010)
49. P. Mulvaney, Langmuir **12**, 788 (1996)
50. S.M. Hosseinpour-mashkani, M. Ramezani, Mater. Lett. **130**, 259 (2014)
51. S. Muthukrishnan, B. Vellingiri, G. Murugesan, Futur. J. Pharm. Sci. **4**, 206 (2018)
52. S. Wei, Y. Wang, Z. Tang, J. Hu, R. Su, J. Lin, T. Zhou, H. Guo, N. Wang, R. Xu, New J. Chem. **44**, 9304 (2020)
53. N. Tarannum, Divya, Y.K. Gautam, RSC Adv. **9**, 34926 (2019)
54. S. Bhowmik, B.K. Datta, A.K. Saha, P. Chakma, N.C. Mandal, Not. Sci. Biol. **8**, 106 (2016)
55. K. Kanagamani, P. Muthukrishnan, M. Ilayaraja, K. Shankar, A. Kathiresan, J. Inorg. Organomet. Polym. Mater. **28**, 702 (2018)
56. D. Sasidharan, T.R. Namitha, S.P. Johnson, V. Jose, P. Mathew, Sustain. Chem. Pharm. **16**, 100255 (2020)
57. S. Ojha, A. Sett, U. Bora, Adv. Nat. Sci. Nanosci. Nanotechnol. **8**, 035009 (2017)
58. S. Priyadarshini, V. Gopinath, N. Meera Priyadharsshini, D. MubarakAli, P. Velusamy, Colloid Surf. B **102**, 232 (2013)
59. S. Soman, J.G. Ray, J. Photochem. Photobiol. B **163**, 391 (2016)
60. B. Adebayo-Tayo, A. Salaam, A. Ajibade, Heliyon **5**, e02502 (2019)
61. Z. Wei, M. Zhou, H. Qiao, L. Zhu, H. Yang, T. Xia, J. Nanomater. **2009**, 5 (2009)
62. G. Franci, A. Falanga, S. Galdiero, L. Palomba, M. Rai, G. Morelli, M. Galdiero, Molecules **20**, 8856 (2015)
63. S. Pal, Y.K. Tak, J.M. Song, Appl. Environ. Microbiol. **73**, 1712 (2007)
64. A. Panáček, L. Kvítek, M. Smékalová, R. Večeřová, M. Kolář, M. Röderová, F. Dyčka, M. Šebela, R. Prucek, O. Tomanec, R. Zbořil, Nat. Nanotechnol. **13**, 65 (2018)
65. S. Medda, A. Hajra, U. Dey, P. Bose, N.K. Mondal, Appl. Nanosci. **5**, 875 (2015)
66. A. Mayer, M. Vadon, B. Rinner, A. Novak, R. Wintersteiger, E. Fröhlich, Toxicology **258**, 139 (2009)
67. J. Choi, V. Reipa, V.M. Hitchins, P.L. Goering, R.A. Malinauskas, Toxicol. Sci. **123**, 133 (2011)
68. L.Q. Chen, L. Fang, J. Ling, C.Z. Ding, B. Kang, C.Z. Huang, Chem. Res. Toxicol. **28**, 501 (2015)
69. D.M.S. Vishnu Kiran Manam, World J. Pharm. Sci. **2**, 926 (2014)
70. K. Kanagamani, P. Muthukrishnan, K. Shankar, A. Kathiresan, H. Barabadi, M. Saravanan, J. Clust. Sci. **30**, 1415 (2019)
71. S.P. Singh, A. Mishra, R.K. Shyanti, R.P. Singh, A. Acharya, Biol. Trace Elem. Res. (2020). <https://doi.org/10.1007/s12011-020-02255-z>
72. R.R. Remya, S.R.R. Rajasree, L. Aranganathan, T.Y. Suman, Biotechnol. Rep. **8**, 110 (2015)
73. M. Sivakumar, S. Surendar, M. Jayakumar, P. Seedeve, P. Sivasankar, M. Ravikumar, M. Anbazhagan, T. Murugan, S.S. Siddiqui, S. Loganathan, J. Clust. Sci. **32**, 167–177 (2020)

Publisher's Note Springer Nature remains neutral with regard to jurisdictional claims in published maps and institutional affiliations.



Bioactive Molecules Coated Silver Oxide Nanoparticle Synthesis from *Curcuma zanthorrhiza* and HR-LCMS Monitored Validation of Its Photocatalytic Potency Towards Malachite Green Degradation

K. S. Aiswariya¹ · Vimala Jose¹

Received: 6 February 2021 / Accepted: 20 May 2021

© The Author(s), under exclusive licence to Springer Science+Business Media, LLC, part of Springer Nature 2021

Abstract

The study focuses on a non-stringent, rapid and sustainable way for the synthesis of silver oxide nanoparticles (Ag₂ONPs) using aqueous rhizome extract of *Curcuma zanthorrhiza* Roxb. (Cz). High resolution liquid chromatography mass spectroscopy (HR-LCMS) was used for the simultaneous identification of bioactive molecules in the aqueous rhizome extract and its biosynthesized nanoparticles. The presence of eleven bioactive molecules in the rhizome extract acts as reducing and capping agents during the synthesis of Ag₂ONPs. The molecules coated to Ag₂ONPs were identified to be majorly sesquiterpenoids and lipid molecules. The analytical techniques used for the nanoparticle characterization included UV–Visible spectrum, which showed SPR band at 409 nm; FTIR spectrum depicted the bioactive molecules involved in capping and reduction of silver ions to silver oxide nanoparticles; XRD pattern attributed to fcc structure of CzAg₂ONPs with an average size of 39.7 nm; HR-TEM and FESEM confirmed the size and morphology of CzAg₂ONPs. The chemical nature of the bioactive molecules bound to Ag₂ONPs revealed by HR-LCMS was in agreement with FTIR spectral data. The CzAg₂ONPs exhibited efficient photocatalytic activity in the degradation of the toxic dye malachite green (MG) as revealed by the absorption spectra. The degraded product was subjected to HR-LCMS and found to be non-toxic. The results revealed the promising potential of bioactive molecules coated Ag₂ONPs for environmental cleanup.

Keywords Aqueous extract · Harminine · Coumarins · Photocatalyst · Benzophenone

Introduction

The tremendous increase in environmental pollution over the years can be attributed to the broad application of dyes in various industries and the imperfections in their removal. Currently, the commercial dyes have become an unavoidable substance in various industries and their management is of global concern. The highest discharge of dye effluents to the aqueous ecosystem, against the acceptable ecological norms are from the textile industry [1]. Residual dyes on reaching water bodies interfere with the sunlight penetration affecting photosynthesis, which eventually disturbs the

ecosystem. Moreover, these effluents are potent toxins and carcinogens [2]. Due to the stability and persistence of the toxic pollutants in the environment, the development of appropriate treatments for the degradation of dye is necessary. The physicochemical techniques involved in the removal of dye from effluents are often very costly and the disposal of concentrated sludge creates a problem [3]. Time consumption and difficulty in degrading complicated dyes are the drawbacks of biological methods. Despite these challenges, the promising potential of nanotechnology enables the exploitation of nanoparticles and nanomaterials in environmental remediation.

Nanotechnology refers to the wide range of technologies and applications that involve the use of particles ranging from a few nanometers to hundreds of nanometers in diameter. Nanoparticles (NPs) have revolutionized the fields of environmental remediation, medicine, material science, chemistry and engineering. They have been exploited in catalysis, sensor technology, imaging, cancer

✉ Vimala Jose
vimalajoseparaemackel@gmail.com

¹ Centre for Bionanotechnology, Research and Post Graduate Department of Botany, St. Thomas' College, University of Calicut, Thrissur, Kerala 680001, India

treatments and site specific drug delivery because of their characteristic high surface to volume ratio compared to their bulk counterparts [4–8]. But the physicochemical processes involved in the synthesis of metallic nanoparticles involves the use of toxic solvents, posing a serious threat to the environment [9]. Therefore, in recent times, the use of natural materials such as microbes, parasites, yeast, seaweeds and plants as basic hotspot for the synthesis of metal nanoparticles has gained considerable interest among researchers [10, 11].

Plants are enriched with bioactive molecules which are unique in structure and function justifying their role in pharmaceutical, biomedical, nutraceutical, cosmeceutical, and chemical industries [12, 13]. Hence, the plants continue to be a critical source of present-day drugs [14–16]. The bioactive molecules have the potential to interact with various other compounds through a variety of chemical reactions. Apart from the pharmaceutical aspects, the tanning activity of plant polyphenols have been exploited in the leather industry [17]. In addition, the antibacterial and chelating capabilities of various plants and phytoplanktons have been used in the treatment of wastewater [18]. Despite the advantages of the biomolecules, the exploitation of the plant resources remains in a nascent stage. Consequently, during the recent years, synthesis of plant-based functional nanoparticles has evolved as a potential area of investigation among the scientific community [19]. Besides, the minimal efforts involved in synthesis, the plant material integrated nanoparticles do not have toxic materials on their surface and also show biocompatibility and biodegradability [20]. Moreover, the bioactive molecules act as reducing and stabilizing agents in the formation of metal nanoparticles [21, 22]. Therefore, the green synthesized nanoparticles have been explored in the field of nanoremediation. The green synthesized silver nanoparticles find its application in the degradation of pesticides, toxic dyes, as environmental sensors and mosquito control along with biological activities [23–31]. In this context, synthesis and application of silver and silver nanoparticle based materials has gained interest due to its morphology, biophysical properties and stability [32, 33].

However, the properties of the green synthesized nanoparticles not only depend on the phytoconstituents present in the plant but also the reaction conditions employed during the synthesis. Although synthesis of metallic nanoparticles utilizing plant's concentrates has been accounted for different plants, such as *Berberis vulgaris*, *Carica papaya*, *Ficus hispida*, *Ricinus communis* var. *carmencita*, *Combretum erythrophyllum*, *Morus indica*, *Mimusops coriacea*, *Zingiber officinale*, *Aspilia plurisetata*, *Caesalpinia pulcherrima*, *Sansevieria roxburghiana*, there is still a wide spectrum of plant metabolites yet to be investigated [34–43]. For instance, the

rhizomes of *Curcuma zanthorrhiza* Roxb. (Cz) which are rich in curcuminoids, terpenoids, alkaloids, flavonoids, tannins, phenols and xanthorhizol, [44], have not yet been exploited in the synthesis of Ag₂ONPs. Moreover, the presence of these bioactive molecules accounts for its medicinal properties such as diuretic, anticancer, antioxidant, antibacterial, antifungal, anti-inflammatory and hepatoprotective effects [45–47].

Based on the above considerations, an attempt has been made to synthesize bioactive molecule coated silver oxide nanoparticles using the aqueous rhizome extract of *Curcuma zanthorrhiza* Roxb. The simultaneous identification of the plant derived biological molecules in the rhizome extract of Cz and the biosynthesized nanoparticles were examined using high resolution liquid chromatography mass spectroscopy (HR-LCMS). Different spectroscopic and electron microscopic techniques were used to characterize the physicochemical properties of the as-synthesized nanoparticles. Moreover, the photocatalytic efficiency of CzAg₂ONPs in the degradation of toxic dye malachite green (MG) was ascertained and the degradation products were subjected to HR-LCMS analysis.

Materials and Methods

Preparation of Plant Extract and Identification of Bioactive Molecules by HR-LCMS

Curcuma zanthorrhiza rhizomes (Fig. 1a) were multiplied from the original germplasm collection from the Regional station of National Bureau of Plant Genetic Resources (NBPGR), Thrissur, Kerala, India. It was cleaned, shade dried, powdered and stored. 10 g of this powder was boiled in 100 mL of deionised water for 30 min and filtered using Whatman No. 1 paper. The filtrate was further centrifuged at 5000 rpm and the supernatant was stored at 4 °C for future experiments.

The aqueous rhizome extract was subjected to bioactive molecule analysis by using high resolution liquid chromatograph mass spectrometer coupled to QTOF (HR-LCMS, Aligent Technologies, USA, 1290 Infinity UPHLC System, 6550 iFunnel QTOFs). The liquid chromatographic conditions employed in the bioactive molecule analysis are listed in Table 1. Mass spectra were generated in positive electrospray ionization mode (ESI).

Biosynthesis of Silver Oxide Nanoparticles (CzAg₂ONPs)

The aqueous rhizome extract was added to 1 mM silver nitrate solution, followed by irradiation of sunlight with continuous stirring for 30 min in Erlenmeyer flask. The

Fig. 1 **a** *Curcuma zanthorrhiza* rhizomes, **b** color change in reaction mixture from yellow to reddish brown indicated formation of Ag₂ONPs— (i) aqueous rhizome extract (yellow); (ii) biosynthesized CzAg₂ONP suspension (reddish brown) and **c** HR-LCMS chromatogram of the aqueous rhizome extract of *C. zanthorrhiza*. The peaks corresponds to bioactive molecules namely, norcotinine (peak 1, m/z = 185.0672), N-(1-deoxy-1-fructosyl) Valine (peak 2, m/z = 262.1308), ethyl 3-methyl-9H-carbazole-9-carboxylic acid (peak 3, m/z = 276.1463), feruperine (peak 4, m/z = 310.1306), gibberellic acid 19 (peak 5, m/z = 367.1526), harmanine (peak 6, m/z = 181.0779), gibberellic acid 3 (peak 7, m/z = 369.1358), obliquin (peak 8, m/z = 254.0829), pteryxin (peak 9, m/z = 369.1359), glechomafuran (peak 10, m/z = 231.14) and sinapoylspermine (peak 11, 391.2872) (Color figure online)

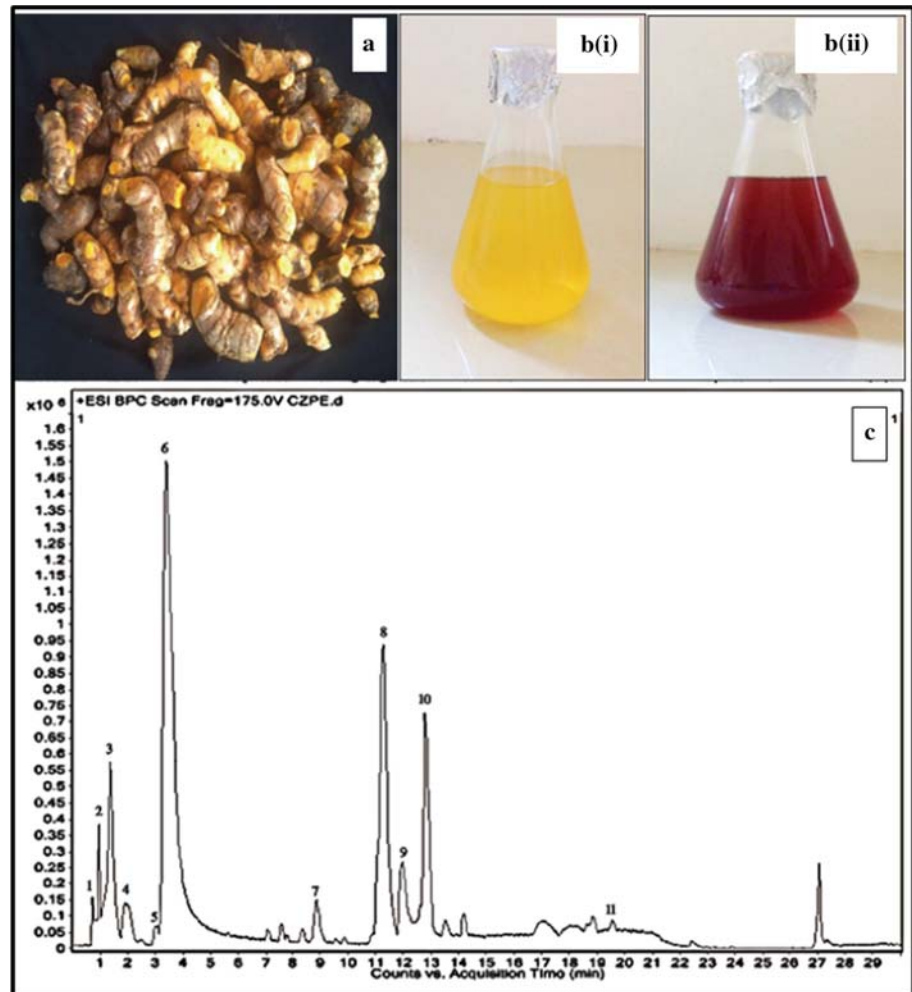


Table 1 Conditions employed during HR-LCMS measurement

Parameter	Condition
Column	Hypersil gold 3 micron, 100*2.1 mm (Aligent 1290 Infinity UHPLC)
Eluent types	90% Acetonitrile/10% water and 0.1% FA
Flow rate (mL min ⁻¹)	0.3
Injection volume (L)	3
Nebulizer pressure (psi)	35
Column temperature (°C)	25
Dry gas flow rate (L min ⁻¹)	13
Dry temperature (°C)	250
Vaporize temperature (°C)	300
Ion source	Positive ESI

ratio of rhizome extract to AgNO₃ was 1:10 by volume. The synthesized CzAg₂ONPs were purified by repeated centrifugation at 12,000 rpm (Eppendorf 5430R) for 20 min followed by dispersion of pellet in deionized water to remove water-soluble biomolecules. The water

suspended nanoparticles were oven dried and were used for all the further studies.

Characterization of Biosynthesized CzAg₂ONPs

The bioreduction of silver ions in the solution was monitored by measuring the UV–Visible spectra of the solution using UV–Visible spectrophotometer (Shimadzu UV probe 1800), at a resolution of 1 nm in the scanning range 600–300 nm using quartz cuvette of path length 1 cm. The X-ray diffraction (XRD) measurements were carried out on a PANalytical X-ray diffractometer at a scanning rate of 20 min⁻¹ with an operating voltage of 40 kV and a current of 15 mA with Cu K α radiation 1.5405 Å monochromatic filter in the angle range $2\theta = 10^\circ$ – 80° . Ultra-thin film of CzAg₂ONPs was prepared by dropping CzAg₂ONP suspension on carbon coated copper grid. It was subsequently analyzed using high-resolution transmission electron microscope (HR-TEM, Tecnai G2, F30) operated at 300 kV was used to analyze the size and morphology of the nanoparticles. The topography of the nanoparticles as well as the elemental composition was studied by field emission scanning electron microscope-energy dispersive analysis of X rays (FESEM EDAX-Supra 55, Karl Zeiss) with an accelerating voltage of 20 kV. The bioactive molecules responsible for the reduction and stabilization of silver ions in the aqueous medium was investigated using FTIR Spectrophotometer (Thermo Nicolet, Avatar 370) with spectral range 4000–400 cm⁻¹, resolution 4 cm⁻¹ and KBr pellets. Further, HR-LCMS spectra of the nanoparticle aqueous suspension was taken and compared against the HR-LCMS spectra of aqueous plant extract to ascertain the bound bioactive molecules in the synthesized nanoparticles.

Photocatalytic Degradation of Malachite Green (MG)

The photocatalytic activity of CzAg₂ONPs in the degradation of MG in aqueous solution was evaluated as a model system for investigating nanoparticle efficiency in removing cationic dyes [1]. The aqueous solution of MG (10 mg L⁻¹) was treated with 100 μ g L⁻¹ of CzAg₂ONPs and kept in dark for 30 min with continuous stirring prior to irradiation. The light source used for the irradiation was sunlight (600–800 μ E m⁻² s⁻¹) and UV lamp (30 W, 253 nm, Philips Holland) for duration of 4 h and 24 h, respectively in two sets of experimental conditions. At regular time intervals, 5 mL suspensions were taken from the two irradiation trials, centrifuged and the absorbance spectra were recorded using UV–Visible spectrophotometer [48]. The percentage of degradation was calculated using,

Percentage degradation = $(C_0 - C)/C_0 \times 100$, C_0 is the concentration of dye prior to the reaction, C is the concentration of dye after the reaction.

MG solution (10 mg L⁻¹) was exposed to same physical conditions to serve as control in the experiment. The degraded products were further analyzed by HR-LCMS, with specified chromatographic conditions (Table 1).

Results and Discussions

Bioactive Molecules Analysis of Aqueous Rhizome Extract

The HR-LCMS analysis revealed the presence of eleven bioactive molecules in the aqueous rhizome extract of CZ (Fig. 1c). The bioactive molecules were identified based upon the spectral similarity with the MS library (NIST MS Search 2.0) and the Human Metabolome Database. The spectrometric data of the bioactive molecules including retention time, molecular mass, molecular formula, adduct ions formed in ion source and peak area percentage are listed in Table 2. The bioactive molecules identified by HR-LCMS analysis were norcotinine (peak 1, $m/z = 185.0672$), N-(1-deoxy-1-fructosyl) Valine (peak 2, $m/z = 262.1308$), ethyl 3-methyl-9H-carbazole-9-carboxylic acid (peak 3, $m/z = 276.1463$), feruperine (peak 4, $m/z = 310.1306$), gibberellic acid 19 (peak 5, $m/z = 367.1526$), harmanine (peak 6, $m/z = 181.0779$), gibberellic acid 3 (peak 7, $m/z = 369.1358$), obliquin (peak 8, $m/z = 254.0829$), pteryxin (peak 9, $m/z = 369.1359$), glechomafuran (peak 10, $m/z = 231.14$) and sinapoylspermine (peak 11, 391.2872) which belonged to the organic class of compounds namely, pyridine derivatives, fructose aminoacids, carbozoles, methoxy phenols, plant hormone, β carboline alkaloids, plant hormone, coumarins, germacrane furano sesquiterpenoids and hydroxycinnamic acid derivatives respectively. The germacrane type of sesquiterpenes are widely reported in the genus *Curcuma* [49]. The peak with m/z 231.14 corresponds to glechomafuran, a germacrane furano sesquiterpenoid, and this type of terpenoid has been reported in the rhizomes of *C. zedoaria* [50]. Hydroxycinnamic acid derivatives were also identified in the rhizomes of *C. domestica* [51]. However, the peak with m/z 391.287 was identified to be sinapoylspermine, a polyamine conjugated hydroxycinnamic acid [52].

The highest peak was identified to be of harminine, a β carboline alkaloid with a peak area of 35.33%, followed by obliquin, glechomafuran, ethyl 3-methyl-9H-carbazole-9-carboxylic acid, pteryxin, N-(1-deoxy-1-fructosyl) Valine, gibberellic acid 3, feruperine, sinapoylspermine, gibberellic acid 19 with peak area of 20%, 8.57%, 6.78%, 5.33%,

Table 2 Bioactive macromolecules in the aqueous rhizome extract of *Curcuma zanthorrhiza* identified from the HR-LCMS chromatogram presented in Fig. 1c

Peak No.	Retention time	Molecular mass (g/mol)	m/z	Formula	Adduct	Compound name	Peak area percentage (%)
1	0.762	162.0772	185.0672	C ₉ H ₁₀ N ₂ O	(M + Na)	Norcotinine (pyridine and derivatives)	0.37
2	1.147	279.134	262.1308	C ₁₁ H ₂₁ NO ₇	(M + H-H ₂ O)	N-(1-deoxy-1-fructosyl)Valine (fructose aminoacid)	3.67
3	1.537	253.1571	276.1463	C ₁₆ H ₁₅ NO ₂	(M + Na)	Ethyl 3-methyl-9H-carbazole-9-carboxylic acid (alkaloid)	6.78
4	1.896	287.1414	310.1306	C ₁₇ H ₂₁ NO ₃	(M + Na)	Feruperine (methoxyphenols)	3.13
5	2.997	362.1739	367.1526	C ₂₀ H ₂₆ O ₆	(M + Na-H ₂ O)	Gibberellic acid 19 (hormone)	0.77
6	3.227	198.0812	181.0779	C ₁₂ H ₁₀ N ₂ O	(M + H-H ₂ O)	Harmanine (alkaloid)	35.33
7	8.818	346.1472	369.1358	C ₁₉ H ₂₂ O ₆	M + Na	Gibberellic acid 3 (hormone)	3.44
8	11.256	244.0757	245.0829	C ₁₄ H ₁₂ O ₄	M + H	Obliquin (coumarins)	20.00
9	11.703	386.1393	369.1359	C ₂₁ H ₂₂ O ₇	M + H-H ₂ O	Pteryxin (coumarins)	5.33
10	12.705	248.1433	231.14	C ₁₂ H ₂₀ O ₃	M + H-H ₂ O	Glechomafuran (germacrane sesquiterpenoids)	8.57
11	19.626	408.2905	391.2872	C ₂₁ H ₃₆ N ₄ O ₂	M + + H-H ₂ O	Sinapoylspermine (hydroxycinnamic acid derivatives)	1.10

3.67%, 3.44%, 3.13%, 1.1% and 0.77% respectively. Norcotinine, a pyrimidine derivative was quantified to be the least component present in the aqueous rhizome extract with an intensity of 0.37%. Moreover, harminine (m/z = 181.0779) was reported to be effective in the synthesis of silver nanoparticles and in pest management [53]. Major properties of bioactive compounds are given in Table 4. Furthermore, the coumarins, obliquin and pteryxin were identified for the first time in the aqueous rhizome extract of *C. zanthorrhiza*.

Biosynthesis of CzAg₂ONPs

Synthesis of CzAg₂ONPs was observed by the addition of aqueous rhizome extract of *Curcuma zanthorrhiza* to 1 mM AgNO₃, kept under sunlight for 30 min. The color of the reaction mixture changed from pale yellow to reddish-brown color after 30 min irradiation, which indicated the formation of Ag₂ONPs at pH 5.65 (Fig. 1b). The excitation of surface vibration plasmon in the silver nanoparticles results in the change in color. A study by Hosseinpour et al., reported the requirement of 180 min for the formation of silver nanoparticles by thermal decomposition method [54]. However, in our study, the formation of Ag₂ONPs occurred more rapidly, where the whole reaction was completed within 30 min in an ambient condition.

Characterization of Biosynthesized CZAg₂ONPs

UV-Visible Spectroscopy

The formation of CzAg₂ONPs was primarily characterized by UV-Visible Spectroscopy. In the UV spectrum, the broadening of peak indicated the particles are polydispersed in aqueous suspension [55]. According to Mie's theory, the absorption spectra of spherical nanoparticles show only a single Surface Plasmon Resonance (SPR) band. In the present study, the formed Ag₂ONPs was confirmed by UV-Visible spectrophotometer analysis. The UV-Visible spectra showed maximum absorption at 409 nm, with a single SPR band (Fig. 3a) revealing the spherical shape of Ag₂ONPs [56, 57]. The λ max of the aqueous rhizome extract was at 272.5 nm (Fig. 2).

X-ray Diffraction (XRD) Analysis

The XRD technique was used to determine and confirm the crystalline structure of Ag₂ONPs. Well defined characteristic diffraction peaks at 32.2, 38.1, 46.2, 54.63, 57.24, 64.98 and 76.54 corresponding to (111), (200), (211), (220), (221), (222) and (311) planes, respectively were identified, attributing to face-centred (fcc) crystal structure of metallic Ag₂ONPs (Fig. 3b). The XRD pattern of the biosynthesized CzAg₂ONPs matched with the standard JCPDS file (No. 76-1393). Dhoondia and Chakraborty

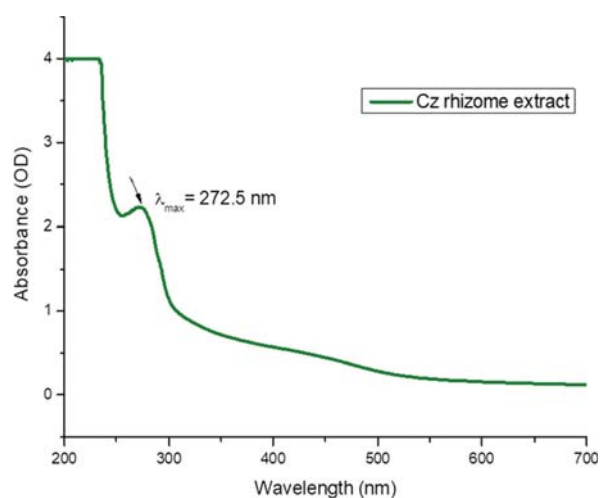


Fig. 2 The UV–Vis absorption spectrum of aqueous rhizome extract of *C. zanthorrhiza* (272.5 nm)

reported a similar finding on the formation of Ag_2ONPs using *Lactobacillus* [58]. In the present study, the average crystallite size calculated using the Scherrer equation for the biosynthesized CzAg_2ONPs were found to be 39.7 nm.

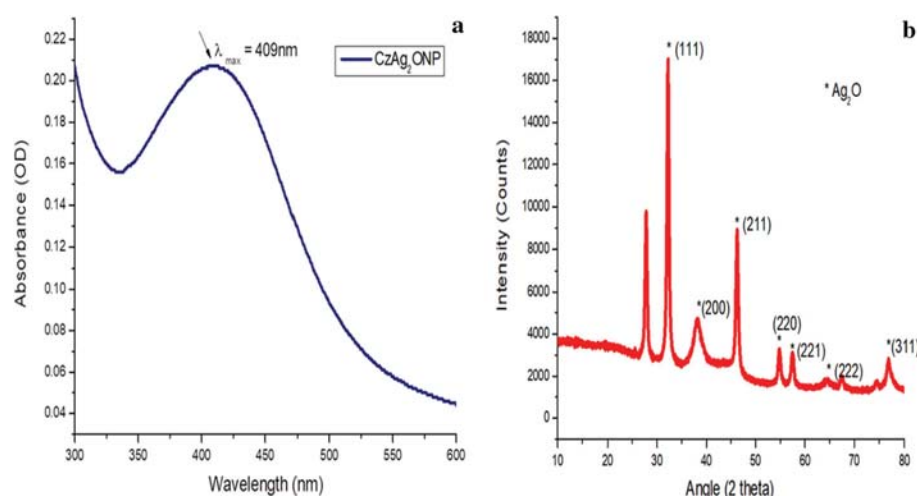
$$D = \frac{k\lambda}{\beta \cos\theta}$$

where D is the average crystallite size, $k = 0.94$, λ is the X ray wavelength, β is the full width at half maxima (FWHM) and θ is the diffraction angle.

Electron Microscopy (HR-TEM and FESEM)

The HR-TEM micrographs revealed the spherical nature of the biosynthesized CzAg_2ONPs , which was in agreement with the UV data. The SAED pattern with bright circular spots indicated (111), (211), (220) and (311) planes and

Fig. 3 a The UV–Vis absorption spectrum of CzAg_2ONPs (409 nm) synthesized with 0.1% (w/v) aqueous rhizome extract containing 1 mM AgNO_3 irradiated under sunlight for 30 min and **b** XRD pattern of CzAg_2ONPs synthesized from the aqueous rhizome extract attributed to fcc structure of metallic Ag_2ONPs with an average crystallite size 39.7 nm



revealed the polycrystalline nature of nanoparticles, which was consistent with the XRD results obtained (Fig. 4b, c). The d spacing value of 0.276 nm observed is in agreement with the (111) lattice spacing of fcc silver ($d_{111} = 0.2748$) which further follows the standard JCPDS file (No. 76-1393). Further insight on the surface morphology of CzAg_2ONPs was obtained from FESEM micrographs. In agreement with the XRD results, the TEM and FESEM micrographs (Fig. 4a) also revealed the synthesized Ag_2ONPs were spherical in shape with a diameter ranging from 17.98 to 46.73 nm.

Energy Dispersive Analysis of X-rays (EDAX)

The EDAX assists in finding out the elemental composition of the synthesized nanoparticles (Fig. 4d). The EDAX spectrum displayed the presence of elemental oxygen, silver with weight percentage 25.2%, 64.24%, respectively and the absence of elemental nitrogen confirming the reduction of silver nitrate to silver oxide nanoparticles. The presence of sharp and intense band peak at 3 keV is typical of the existence of metallic silver. Presence of signals for carbon in the spectrum is because of the biomolecules found in the rhizome extract that had been related with the synthesis of CzAg_2ONPs .

Fourier Transform Infrared (FTIR) Spectroscopy

The FTIR spectroscopic peaks showed the bioactive molecules in the aqueous rhizome extract responsible for the reduction of silver ions to metallic silver oxide nanoparticles, with prominent peaks at 3467.654, 2075.133, 1631.563, and 561.2115 cm^{-1} (Fig. 5). The spectrum showed the intense and broad absorption peak at 3467.654 denoting O–H stretching [29]. A strong and sharp

Fig. 4 **a** FESEM image of CzAg_2ONPs biosynthesized from the aqueous rhizome extract denoting the spherical nature of the nanoparticles, **b** HR-TEM image of biosynthesized CzAg_2ONPs revealed its spherical nature with size ranging from 17.98 to 46.73 nm, **c** SAED pattern attributing to the polycrystalline nature of CzAg_2ONPs and **d** EDAX image of CzAg_2ONPs

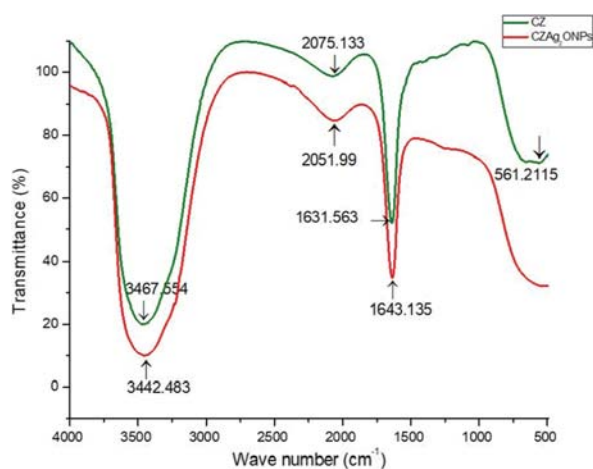
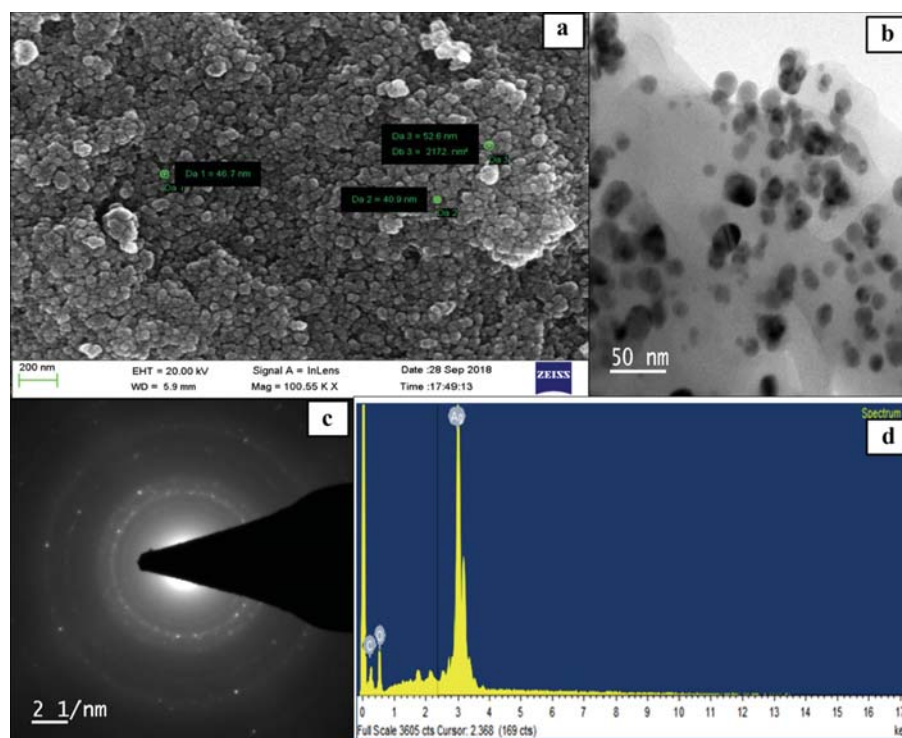


Fig. 5 FTIR spectra of the aqueous rhizome extract (CZ) and biosynthesized CzAg_2ONPs with spectral range 4000–400 cm^{-1}

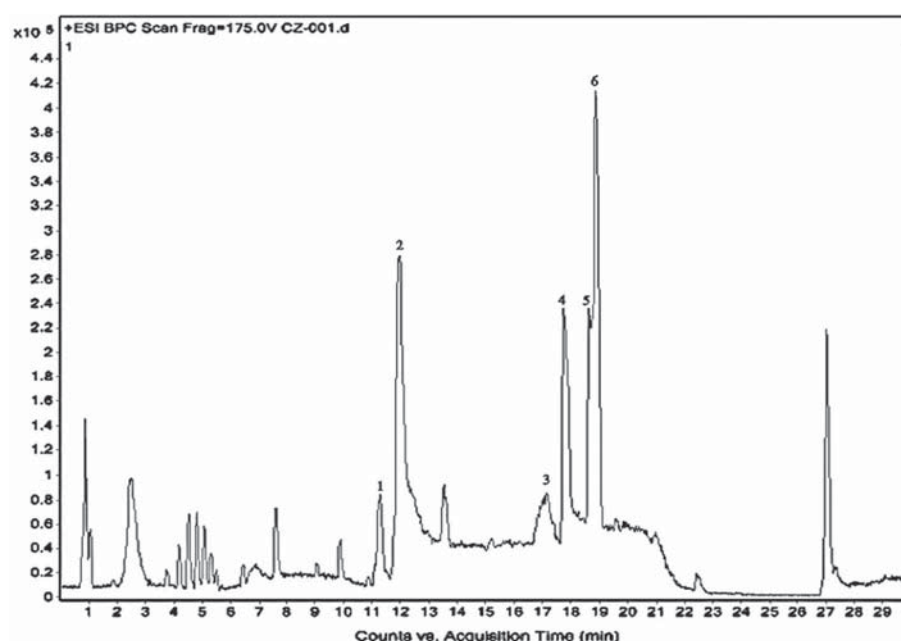
absorption band at 1631.563 cm^{-1} can be assigned to the stretching vibration of (NH) C=O group. Mariselvam et al. reported a similar finding which indicated the formation silver nanoparticles capped with biomolecules from the absorption band at 1638 cm^{-1} [59]. Furthermore, the peaks at 2075.133 and 561.2115 cm^{-1} indicated the alkyne group in rhizome extract and C–Br stretching, respectively. For the biosynthesized CzAg_2ONPs , the characteristic bands were at 3442.483, 2051.99, 1643.135 cm^{-1} and absence of

band around 500 cm^{-1} . There was a large shift in the peaks observed in CzAg_2ONPs , 3467.654 to 3442.483 cm^{-1} , 2075.133 to 2051.99 cm^{-1} , 1631.563 to 1643.135 cm^{-1} which indicated the involvement of hydroxyl groups, carboxyl amines, amino acid residues and alkyne derivatives which corresponds to carbohydrates, proteins and phenols, respectively. The bioactive molecules identified in the aqueous rhizome extract are listed in Table 2. However, from the IR spectrum results, it can be attributed that some of these bioactive molecules are involved in the reduction of silver nitrate to silver oxide nanoparticles [60, 61]. It is also reported that the biomolecules play a major role in reduction of gold chloride and capping with polymers improve their properties [62]. The amide linkage of proteins could be likely to form a coat over the CzAg_2ONPs , stabilizing them in the aqueous medium [63].

High Resolution Liquid Chromatography Mass spectroscopy (HR-LCMS)

The presence of six bioactive molecules were ascertained in the CzAg_2ONP aqueous suspensions using the HR-LCMS analysis (Fig. 6) and these compounds were comparable with the HR-LCMS data of the aqueous rhizome extract (Fig. 1c). The bioactive molecules bound to Ag_2ONPs were zedorone (peak 2, $m/z = 229.1244$), glechomafuran (peak 4, $m/z = 231.1398$) which belonged to

Fig. 6 HR-LCMS chromatogram of the biosynthesized silver oxide nanoparticle suspension. The bound bioactive molecules on CzAg₂ONPs were tripeptide Val–His–Arg (peak 1, m/z = 415.217), zedorone (peak 2, m/z = 229.1244), 1-hexadecanoyl-sn-glycerol (peak 3, m/z = 313.2763), glechomafuran (peak 4, m/z = 231.1398), dihydrosphingosine (peak 5, m/z = 284.2973), and 1-octadecanoyl-rac-glycerol (peak 6, m/z = 341.3073)



germacrene sesquiterpenoids, an aminoalcohol dihydrosphingosine (peak 5, m/z = 284.2973), two lipid molecules namely palmitoyl glycerol (1-hexadecanoyl-sn-glycerol) (peak 3, m/z = 313.2763), stearoyl glycerol (1-octadecanoyl-rac-glycerol) (peak 6, m/z = 341.3073) and tripeptide Val–His–Arg (peak 1, m/z = 415.217) and were quantified to 15.04%, 8.79%, 8.17%, 10.55%, 14.28% and 3.51%, respectively. The retention time, adduct ions formed in ion source, molecular mass, molecular formula and peak area percentage of the bioactive molecules are listed in Table 3. This result ascertains the presence of

bound bioactive molecules in the biosynthesized CzAg₂ONPs which corroborates with the FTIR results.

Photocatalytic Degradation of MG

The drop in the characteristic absorption peak of MG at 615 nm was used as an indicator for examining the degradation of the dye catalyzed by CzAg₂ONPs. There was a gradual decrease in the main absorption peak of MG with the increase in exposure time to sunlight and UV light (Fig. 7a, b). The sunlight exposed dye-nanoparticle

Table 3 Bioactive macromolecules coated on CzAg₂ONPs identified from the HR-LCMS Chromatogram presented in Fig. 6

Peak No	Retention time	Molecular mass (g/mol)	m/z	Formula	Adduct	Compound name	Peak area percentage (%)
1	11.8	410.236	415.217	C ₁₇ H ₃₀ N ₈ O ₄	(M + Na-H ₂ O)	Val–His–Arg (tripeptide)	3.51
2	12.245	246.129	229.124	C ₁₅ H ₁₈ O ₃	(M + H-H ₂ O)	Zedorone (Germacrane sesquiterpenoids)	15.04
3	17.332	330.279	313.276	C ₁₉ H ₃₈ O ₄	(M + H-H ₂ O)	1-hexadecanoyl-sn-glycerol	10.55
4	17.734	248.143	248.297	C ₁₅ H ₂₀ O ₃	(M + H-H ₂ O)	Glechomafuran (Germacrane sesquiterpenoids)	8.79
5	18.641	301.300	284.297	C ₁₈ H ₃₉ NO ₂	(M + H-H ₂ O)	Dihydrosphingosine (aminoalcohol)	8.17
6	18.82	358.310	341.307	C ₂₁ H ₄₂ O ₄	(M + H-H ₂ O)	1-octadecanoyl-rac-glycerol	14.28

The phytoconstituents were identified based upon spectral similarity with the MS library (NIST MS Search 2.0) and the Human Metabolome Database

suspension had quick de-colorization (4 h) compared to UV light (24 h) exposed suspension. The percentage of

degradation of MG was 94.7% under sunlight and 22.83% upon UV irradiation.

Fig. 7 UV–Visible spectra of decomposition of MG dye using CzAg₂ONPs as photocatalysts: **a** under sunlight (94.7% degradation) **b** under UV light (22.83% degradation), **c** HR-LCMS chromatogram of MG treated with CzAg₂ONPs after irradiation with sunlight and **d** its degradation products—(1) 4-amino benzoic acid (m/z 137.04, 1.08%), (2) phenylacetic acid (m/z 192.09, 7.99%), (3) N,N' diacetyl 1,4 phenylene diamine (m/z 192.09, 11.46%), (4) methyl 3,4 di amino benzoate (m/z 166.07, 4.85%), (5) 4-methyl amino benzoic acid (m/z 151.06, 11.43%), (6) 4,4' diamino benzophenone (m/z 212.09, 6.89%), (7) 4-amino benzophenone (m/z 197.08, 0.75%) and (8) 4,4' methylene bis (N,N'dimethyl) benzamine (m/z 254.18, 11.09%)

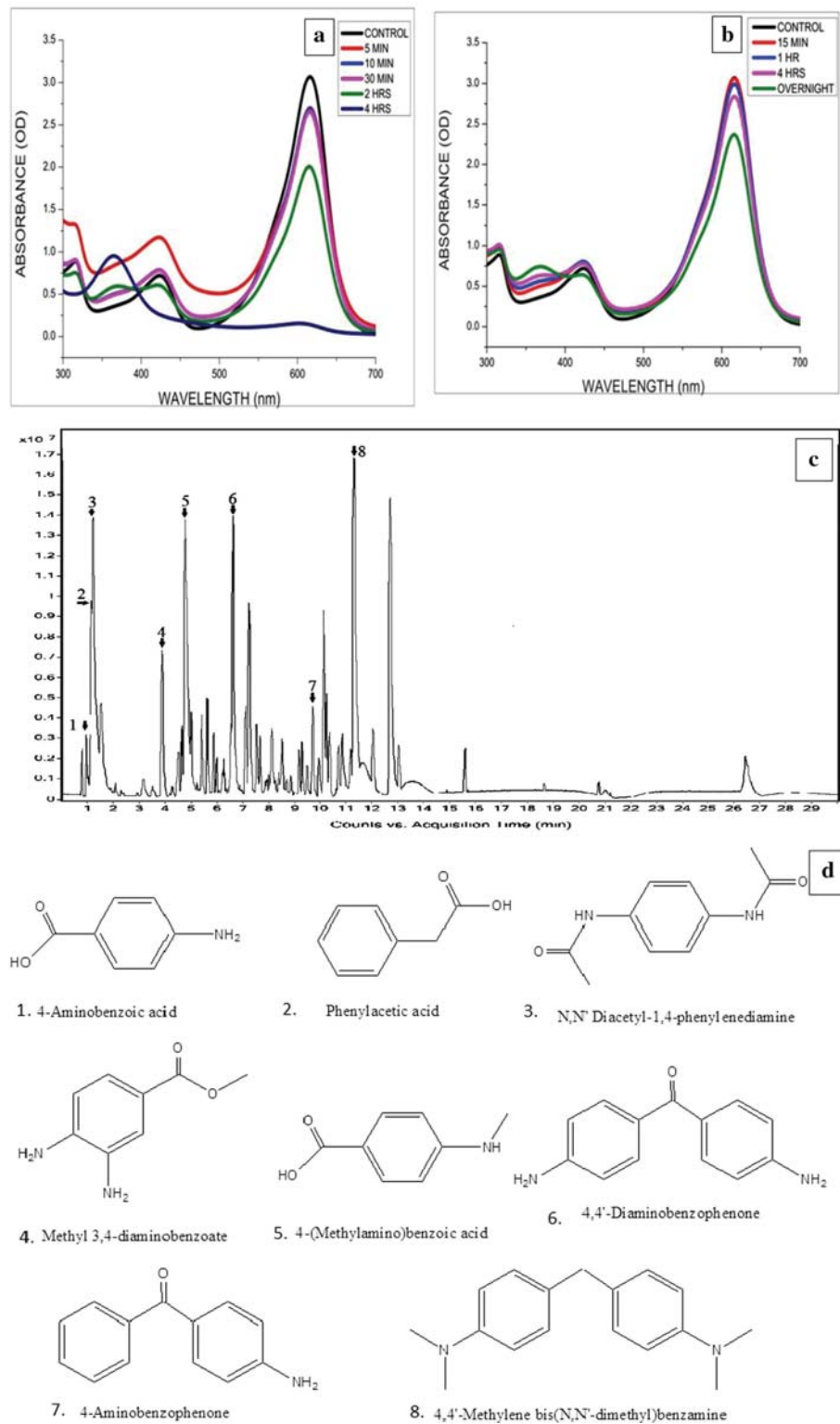


Table 4 Bioactive compounds and their properties

Bioactive Compounds	Properties	References
Norcotinine	Neuropharmacological property	[68]
Feruperine	Antioxidant activity	[69]
Harmanine	Insecticidal property	[53]
Obliquin	Anti-depressive activity	[70]
Pteryxin	Vasorelaxant, hepatoprotective, treatment of Alzheimer's disease	[71]
Glechomafuran	Antioxidant, anticancer activity	[72]
Sinapoylspermine	Anti-inflammatory, neuroprotective, antioxidant, anticancer, antimicrobial, cosmetic	[73]
Zedorone	Antioxidant, anticancer, antimicrobial, carminative, analgesic, insecticide	[74]

The degradation product when subjected to HR-LCMS analysis displayed the possible intermediates formed during the breakdown of MG. The retention time of the control dye MG is at 11.585, which was different from the retention time of all the degraded products in the range of 1.02–11.447 (Fig. 7c). The HR-LCMS analysis of MG and degradation products confirmed the efficacy of bioactive molecule coated CzAg₂ONPs as good photocatalysts in the effective removal of the model dye. The reaction showed no progress in the absence of nanocatalysts (control). The HR-LCMS analysis of reaction product of MG-nanoparticle suspension showed the presence of compounds with molecular weights 137.04, 136.03, 192.09, 166.07, 151.06, 212.09, 197.08 and 254.18 m/z which could be interpreted as structures of 4-aminobenzoic acid, phenylacetic acid, N, N' diacetyl 1,4 phenylene diamine, methyl 3,4 diaminobenzoate, 4-methyl aminobenzoic acid, 4,4' diamino benzophenone, 4-amino benzophenone and 4,4' methylene bis (N,N'dimethyl) benzamine, respectively (Fig. 7d), whereas the molecular weight of MG dye is 330.20 m/z. Out of the eight intermediates formed during the breakdown of MG, N,N' diacetyl 1,4 phenylene diamine was quantified to be the most abundant degradation product (11.46%), followed by 4-methyl aminobenzoic acid (11.43%), 4,4' methylene bis (N,N' dimethyl) benzamine (11.09%), phenylacetic acid (7.99%), 4,4' diamino benzophenone (4.85%), 4-aminobenzoic acid (1.08%) and 4-amino benzophenone (0.75%).

The formation of benzophenone derivatives by N-demethylation of MG have been reported as one of the major reaction involved in photo-oxidative process [64]. This is in agreement with our obtained results, since most of the products identified after degradation was derivatives of benzophenone. The possible mechanism of degradation may be due to the generation of hydroxyl radicals by the highly energetic electrons released when the photons struck the valence electrons of the molecule capped CzAg₂ONPs [65]. These low molecular weight structures being mostly

benzene derivatives may further be decomposed to form small organic molecules which eventually breaks down into CO₂ and H₂O [66]. Moreover, the formation of highly toxic leucomalachite green, a reduced form of MG was not detected in our study ascertaining the non-toxic dye removal process by bioactive molecule coated CzAg₂ONPs, rendering unhazardous products to the environment [67] (Table 4).

Conclusion

The promising potential of the aqueous rhizome extract of *Curcuma zanthorrhiza* was for the first time exploited in a non-stringent and sustainable way for the synthesis of bioactive molecule coated silver oxide nanoparticles. The bioactive molecules present in the aqueous rhizome extract were identified by HR-LCMS analysis. The analytical capabilities of different spectroscopic techniques like UV–Visible Spectroscopy, FTIR, XRD and HR-LCMS were used to detect, identify, quantify and characterize the nanoparticles. The size and morphology of the nanoparticles were ascertained by HR-TEM and FESEM-EDAX. Among the different available analytical tools used for the characterization of biosynthesized nanoparticles, HR-LCMS offers remarkable capacities for the identification and quantification of associated molecules in the nanoparticles. The CzAg₂ONPs proved outstanding photocatalytic efficacy in the debasement of toxic dye, MG. HR-LCMS analysis indicated degradation of MG after the CzAg₂ONP treatment, whereas no change of MG was found in the control. By integrating HR-LCMS with the UV–Visible Spectroscopy, conclusive evidences were achieved for the photocatalytic degradation of MG, ultimately formulating a bioremediation protocol. Therefore, the results proved promising potential of *Curcuma zanthorrhiza* derived bioactive molecule coated Ag₂ONPs in the degradation of MG. Further, we could also develop a

simple and sensitive HR-LCMS mediated protocol for the detection and quantification of molecules in the nanoparticles and its degradation products.

Acknowledgements We gratefully acknowledge Council of Science and Industrial Research (CSIR) [File No. 08/633(0005)/2017-EMR-1], Government of India for the fellowship; DST-FIST for the facilities at St. Thomas' College (Autonomous), Thrissur, Kerala, India; SAIF at IIT Bombay, India for HR-TEM and LCMS measurements; Centre for Nanoscience and Nanotechnology, Sathyabama University, Chennai, Tamil Nadu, India for FESEM measurements; STIC Cochin University, Kerala, India for FTIR analysis and Kerala Veterinary and Animal Science University, Thrissur, Kerala, India for Lyophilisation technique.

Author Contributions AKS: Methodology, formal analysis, investigation, data curation, validation, software, writing—original draft. VJ: Conceptualisation, supervision, visualisation, writing—review and editing.

Funding No funds, grants or other support was received.

Declaration

Conflict of interest The authors have no conflict of interest to declare that are relevant to the content of this article.

References

1. X. Wang, Y. F. Zheng, H. Y. Yin, and X. C. Song (2011). *J. Nanosci. Nanotechnol.* **11**, 2501.
2. F. Deniz and R. Kepekci (2017). *Microchem. J.* **132**, 172.
3. T. Robinson, G. McMullan, R. Marchant, and P. Nigam (2001). *Bioresour. Technol.* **77**, 247.
4. N. Norouzi, M. K. Das, A. J. Richard, A. A. Ibrahim, H. M. El-Kaderi, and S. El-Shall (2020). *Nanoscale* **12**, 19191.
5. P. Proposito, L. Burratti, and I. Venditti (2020). *Chemosensors* **8**, 1.
6. L. L. Israel, A. Galstyan, E. Holler, and J. Y. Ljubimova (2020). *J. Control. Release* **320**, 45.
7. F. Ren, H. Liu, H. Zhang, Z. Jiang, B. Xia, C. Genevois, T. He, M. Allix, Q. Sun, Z. Li, and M. Gao (2020). *Nano Today* **34**, 100905.
8. M. Gisbert-Garzarán, J. C. Berkmann, D. Giasafaki, D. Lozano, K. Spyrou, M. Manzano, T. Steriotis, G. N. Duda, K. Schmidt-Bleek, G. Charalambopoulou, and M. Vallet-Regí (2020). *ACS Appl. Mater. Interfaces* **12**, 14946.
9. K. D. Lee and P. C. Nagajyothi (2011). *J. Nanomater.* **2011**, 557.
10. P. B. Dayma, A. V. Mangrola, S. P. Suriyaraj, P. Dudhagara, and K. Rajesh (2019). *J. Pharm. Chem. Biol. Sci.* **7**, 94.
11. S. Mohan, O. S. Oluwafemi, S. P. Songca, V. P. Jayachandran, D. Rouxel, O. Joubert, N. Kalarikkal, and S. Thomas (2016). *J. Mol. Liq.* **213**, 75.
12. M. Bilal and H. M. N. Iqbal (2020). *Int. J. Biol. Macromol.* **151**, 1.
13. S. M. Amini (2019). *Mater. Sci. Eng. C* **103**, 109809.
14. P. J. Delaquis, K. Stanich, B. Girard, and G. Mazza (2002). *Int. J. Food Microbiol.* **74**, 101.
15. R. H. Liu (2003). *Am. J. Clin. Nutr.* **78**, 3.
16. S. E. Cross, Y. S. Jin, Q. Y. Lu, J. Rao, and J. K. Gimzewski, Nanotechnology **22**, (2011).
17. S. Quideau, D. Deffieux, C. Douat-Casassus, and L. Pouységu (2011). *Angew. Chem. Int. Ed.* **50**, 586.
18. O. OoKolawole, S. Oguntoye, O. Agbede, and A. Olayemi (2006). *Ethnobot. Leaflet.* **10**, 228.
19. C. L. Criado (2015). *J. Nanomed. Res.* **2**, 2.
20. M. Ovais, A. T. Khalil, A. Raza, M. A. Khan, I. Ahmad, N. U. Islam, M. Saravanan, M. F. Ubaid, M. Ali, and Z. K. Shinwari (2016). *Nanomedicine* **12**, 3157.
21. R. M. H. Shoker (2020). *Int. J. Res. Appl. Sci. Biotechnol.* **7**, 354.
22. N. Anwar, A. Khan, M. Shah, A. Azam, K. Zaman, and Z. Parven (2016). *Russ. J. Phys. Chem. A* **90**, 2625.
23. N. A. Ramos-Delgado, L. Hinojosa-Reyes, I. L. Guzman-Mar, M. A. Gracia-Pinilla, and A. Hernández-Ramírez (2013). *Catal. Today* **209**, 35.
24. U. Kamran, H. N. Bhatti, M. Iqbal, S. Jamil, and M. Zahid (2019). *J. Mol. Struct.* **1179**, 532.
25. T. Rasheed, F. Nabeel, M. Bilal, and H. M. N. Iqbal (2019). *Biocatal. Agric. Biotechnol.* **19**, 101154.
26. K. Farhadi, M. Forough, R. Molaei, S. Hajizadeh, and A. Rafipour (2012). *Sens. Actuators B Chem.* **161**, 880.
27. K. B. A. Ahmed, R. Senthilnathan, S. Megarajan, and V. Anbazhagan (2015). *J. Photochem. Photobiol. B Biol.* **151**, 39.
28. K. Velayutham, R. Ramanibai, and M. Umadevi (2016). *J. Basic Appl. Zool.* **74**, 37.
29. D. A. Aina, O. Owolo, A. Lateef, F. O. Aina, and A. S. Hakeem (2019). *Karbala Int. J. Mod. Sci.* **5**, 2.
30. M. Arshad, A. Khan, Z. H. Farooqi, M. Usman, M. Abdul Waseem, S. A. Shah, and M. Khan (2018). *Mater. Sci. Pol.* **36**, 21.
31. K. S. Aiswariya and V. Jose (2021). *J. Inorg. Organomet. Polym. Mater.* <https://doi.org/10.1007/s10904-021-01951-0>.
32. A. Syafiuddin, Salmiati, M. R. Salim, A. Beng Hong Kueh, T. Hadibarata, and H. Nur (2017). *J. Chin. Chem. Soc.* **64**, 732.
33. L. P. Silva, T. M. Pereira, and C. C. Bonatto, *Frontiers and Perspectives in the Green Synthesis of Silver Nanoparticles* (Elsevier Inc., Amsterdam, 2019).
34. M. Behravan, A. Hossein Panahi, A. Naghizadeh, M. Ziaee, R. Mahdavi, and A. Mirzapour (2019). *Int. J. Biol. Macromol.* **124**, 148.
35. A. V. Ramesh, D. R. Devi, G. R. Battu, and K. Basavaiah (2018). *S. Afr. J. Chem. Eng.* **26**, 25.
36. S. Ojha, A. Sett, and U. Bora (2017). *Adv. Nat. Sci. Nanosci. Nanotechnol.* **8**, 035009.
37. O. T. Jemilugba, E. H. M. Sakho, S. Parani, V. Mavumengwana, and O. S. Oluwafemi (2019). *Colloids Interface Sci. Commun.* **31**, 100191.
38. S. Some, O. Bulut, K. Biswas, A. Kumar, A. Roy, I. K. Sen, A. Mandal, O. L. Franco, İ. A. İnce, K. Neog, S. Das, S. Pradhan, S. Dutta, D. Bhattacharjya, S. Saha, P. K. Das Mohapatra, A. Bhuimali, B. G. Unni, A. Kati, A. K. Mandal, M. D. Yilmaz, and I. Ocsoy (2019). *Sci. Rep.* **9**, 1.
39. C. R. B. Lopes and L. C. Courrol (2018). *J. Lumin.* **199**, 183.
40. A. R. M. Abd El-Aziz and M. R. Al-Othman (2019). *Pakistan J. Bot.* **51**, 443.
41. A. O. Nyabola, P. G. Kareru, E. S. Madivoli, S. I. Wanakai, and E. G. Maina (2020). *J. Inorg. Organomet. Polym. Mater.* **30**, 3493.
42. P. Moteriya and S. Chanda (2020). *J. Inorg. Organomet. Polym. Mater.* **30**, 3920.
43. A. G. Rama Krishna, C. S. Espenti, Y. V. Rami Reddy, A. Obbu, and M. V. Satyanarayana (2020). *J. Inorg. Organomet. Polym. Mater.* **30**, 4155.
44. H. P. A. Mary, G. K. Susheela, S. Jayasree, A. M. Nizzy, B. Rajagopal, and S. Jeeva (2012). *Asian Pac. J. Trop. Biomed.* **2**, S637.
45. C. Singgih Wahono, C. Diah Setyorini, H. Kalim, N. Nurdiana, and K. Handono (2017). *Int. J. Rheumatol.* **2017**, 1.

46. Y. H. Cheah, F. J. Nordin, R. Sarip, T. T. Tee, H. L. P. Azimahtol, H. M. Sirat, B. A. A. Rashid, N. R. Abdullah, and Z. Ismail (2009). *Cancer Cell Int.* **9**, 1.
47. S. Anjusha and A. Gangaprasad (2014). *J. Pharmacogn. Phytochem.* **3**, 50.
48. T. J. I. Edison and M. G. Sethuraman (2012). *Process Biochem.* **47**, 1351.
49. W. Sun, S. Wang, W. Zhao, C. Wu, S. Guo, H. Gao, H. Tao, J. Lu, Y. Wang, and X. Chen (2017). *Crit. Rev. Food Sci. Nutr.* **57**, 1451.
50. H. Shibuya, Y. Cai, I. Kitagawa, and Y. Hamamoto (1987). *Chem. Pharm. Bull.* **35**, 924.
51. D. Herebian, J. H. Choi, A. M. Abd El-Aty, J. H. Shim, and M. Spitteller (2009). *Biomed. Chromatogr.* **23**, 951.
52. J. Luo, C. Fuell, A. Parr, L. Hill, P. Bailey, K. Elliott, S. A. Fairhurst, C. Martin, and A. J. Michael (2009). *Plant Cell* **21**, 318.
53. A. A. Almadiy, G. E. Nenaah, and D. M. Shower (2018). *J. Pest Sci. (2004)* **91**, 727.
54. S. M. Hosseinpour-mashkani and M. Ramezani (2014). *Mater. Lett.* **130**, 259.
55. S. Bhowmik, B. K. Datta, A. K. Saha, P. Chakma, and N. C. Mandal (2016). *Not. Sci. Biol.* **8**, 106.
56. W. Chengzheng, W. Jiazhi, C. Shuangjiang, M. K. Swamy, U. R. Sinniah, M. S. Akhtar, and A. Umar (2018). *J. Nanosci. Nanotechnol.* **18**, 3673.
57. W. R. Rolim, M. T. Pelegrino, B. de Araújo Lima, L. S. Ferraz, F. N. Costa, J. S. Bernardes, T. Rodrigues, M. Brocchi, and A. B. Seabra (2019). *Appl. Surf. Sci.* **463**, 66.
58. Z. H. Dhoondia and H. Chakraborty (2012). *Nanomater. Nanotechnol.* **2**, 15.
59. R. Mariselvam, A. J. A. Ranjitsingh, C. Thamaraiselvi, and S. Ignacimuthu (2019). *J. King Saud Univ. Sci.* **31**, 1363.
60. S. P. Dubey, M. Lahtinen, and M. Sillanpää (2010). *Process Biochem.* **45**, 1065.
61. R. Mata, J. Reddy Nakkala, and S. Rani Sadras (2015). *Mater. Sci. Eng. C* **51**, 216.
62. N. Anwar, J. Wahid, J. Uddin, A. Khan, M. Shah, S. A. Shah, F. Subhan, M. A. Khan, K. Ali, M. Rauf, and M. Arif (2021). *Vitr. Cell. Dev. Biol. Plant* **57**, 248.
63. S. Priyadarshini, V. Gopinath, N. Meera Priyadharshini, D. Mubarak Ali, and P. Velusamy (2013). *Colloid Surf. B* **102**, 232.
64. L. A. Pérez-Estrada, A. Agüera, M. D. Hernando, S. Malato, and A. R. Fernández-Alba (2008). *Chemosphere* **70**, 2068.
65. L. Wang, F. Lu, Y. Liu, Y. Wu, and Z. Wu (2018). *J. Mol. Liq.* **263**, 187.
66. Y. M. Ju, S. G. Yang, Y. C. Ding, C. Sun, C. G. Gu, Z. He, C. Qin, H. He, and B. Xu (2009). *J. Hazard. Mater.* **171**, 123.
67. S. S. Sutar, P. J. Patil, A. S. Tamboli, D. N. Patil, O. A. Apine, and J. P. Jadhav (2019). *Biocatal. Agric. Biotechnol.* **20**, 101183.
68. P. A. Crooks, M. Li, and L. P. Dvoskin (1997). *Drug Metab. Dispos.* **25**, 47.
69. N. Nakatani, R. Inatani, H. Ohta, and A. Nishioka (1986). *Environ. Health Perspect.* **67**, 135.
70. H. M. P. Poumale, R. Hamm, Y. Zang, Y. Shiono, and V. Kuate, *Coumarins and Related Compounds from the Medicinal Plants of Africa* (Elsevier, Amsterdam, 2013).
71. I. E. Orhan, F. S. Senol, S. Shekfeh, K. Skalicka-Wozniak, and E. Banoglu (2017). *Food Chem. Toxicol.* **109**, 970.
72. L. Quassinti, M. Bramucci, G. Lupidi, L. Barboni, M. Ricciutelli, G. Sagratini, F. Papa, G. Caprioli, D. Petrelli, L. A. Vitali, S. Vittori, and F. Maggi (2013). *Food Chem.* **138**, 808.
73. M. Roumani, R. E. Duval, A. Ropars, A. Risler, C. Robin, and R. Larbat (2020). *Biomed. Pharmacother.* **131**, 110762.
74. M. Soonwera, O. Wongnet, and S. Sittichok (2018). *Phytomedicine* **47**, 93.

Publisher's Note Springer Nature remains neutral with regard to jurisdictional claims in published maps and institutional affiliations.



Green synthesis of silver nanoparticles using *Annona squamosa* L. seed extract: characterization, photocatalytic and biological activity assay

Vimala Jose¹ · Lidiya Raphel¹ · K. S. Aiswariya¹ · Paulson Mathew²

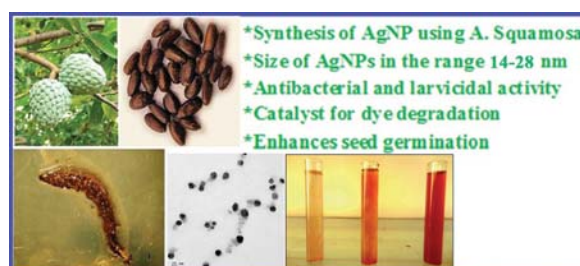
Received: 28 February 2021 / Accepted: 23 March 2021

© The Author(s), under exclusive licence to Springer-Verlag GmbH Germany, part of Springer Nature 2021

Abstract

The aqueous seed extract of *Annona squamosa* L. was used as a reducing and stabilizing agent for the synthesis of silver nanoparticles (AgNPs). The formation of AgNPs in aqueous silver nitrate solution after the addition of the extract was indicated by a colour change from pale yellow to dark brown corresponding to a λ_{\max} at 430 nm. The phytochemicals in the extract, responsible for efficient capping and stabilization of the nanoparticles, were identified by FTIR. Powder XRD pattern demonstrated the polycrystalline nature of the AgNPs. TEM image confirmed that AgNPs were spherical in shape and the average particle size was found to be 22 nm. Further, the nanoparticles exhibited good catalytic activity towards the degradation of coomassie brilliant blue dye and demonstrated significant antibacterial activity. Their larvicidal activity against mosquito larvae showed a LC_{50} value 22.44 $\mu\text{g}/\text{mL}$ against III instars. In addition, AgNPs positively influenced the germination of chickpea seeds.

Graphic abstract



Keywords Silver nanoparticles · *Annona squamosa* L. · Photocatalysis · Bioactivity

Introduction

Nanoparticles are made up of atomic aggregations which are spherical or quasi-spherical structures with 1–100 nm in diameter. When compared to conventional physical or

chemical processes for the preparation of nanoparticles, green methods have a greater number of benefits. Their main advantage is the lack of impact on the environment, as the methods are in line with the principles of green chemistry and the process is cost-effective. Another advantage is the easy transfer of the process to an industrial scale. Due to their medicinal and antimicrobial properties [1], silver nanoparticles (AgNPs) are incorporated in many consumer products and have become one of the most commercialised nanoparticles [2].

Various plant species had been investigated for the synthesis of AgNPs [3] and such nanoparticles possess promising antibacterial properties [4]. For instance, nanoparticles

✉ Paulson Mathew
paulson.org@gmail.com

¹ Department of Botany, Centre for Biotechnology, St. Thomas College (Autonomous), University of Calicut, Thrissur, Kerala 680001, India

² Department of Chemistry, Centre for Sustainability Science, St. Thomas College (Autonomous), University of Calicut, Thrissur, Kerala 680001, India

of silver are effective in inhibiting the growth of both gram-positive and gram-negative bacteria [5–7]. With the rise in antibiotic resistance and the development of new antibiotics, research has begun to focus on these antibacterial nanoparticles as potential new medical tools. Silver is generally used in the nitrate form to induce an antimicrobial effect, but when silver nanoparticles are used, there is a huge increase in the surface area available for the microbe to be exposed to. Bactericidal effects of silver nanoparticles have been documented against bacterial strains such as *Staphylococcus aureus*, *Pseudomonas aeruginosa*, *Escherichia coli*, *Bacillus cereus*, *Listeria innocua*, *Salmonella Choleraesuis* [8–10]. Silver nanoparticles have also been used as optical sensors for the formation of small-molecule adsorbates [11].

Excessive usage of conventional chemicals and pesticides in land and water resources causes many risks to people and the environment. Silver nanoparticles and their composites show improved catalytic activities in dye reduction and removal [12] as documented for organic dyes using *Trigonella foenum-graecum* seeds [13], methyl orange using *Ulva lactuca* [14]. The colloidal solution of silver nanoparticles was found to exhibit mosquito larvicidal activity against dengue and filariasis vector [15]. Larvicidal activity of AgNPs has been studied using *Leucas aspera* [16], *Belosynopsis kewensis* [17], *Excoecaria agalloch* [18] and *Ficus racemosa* [19]. Among the different metal nanoparticles, AgNPs are known to be positively influencing seed-germination process. To date, there are only a few reports on the impact of AgNPs to promote the growth and seed germination [20].

Annona squamosa L., the sugar apple which belongs to the *Annonaceae* family was selected for the present study. *Annonaceae*, plant family commonly named as custard apple family is marked for many medicinal properties such as anti-ulcer, anti-convulsant and antibacterial activity. The plant also possesses analgesic, anti-inflammatory, anti-microbial, cytotoxic, anti-oxidant, anti-lipidemic, molluscicidal, genotoxic, vasorelaxant, anti-tumour, hepatoprotective, larvicidal, insecticidal and anthelmintic properties [21]. The roots, leaves and seeds of *A. squamosa* have several medicinal properties [22]. The active fraction isolated from *A. squamosa* seed extract has strong antibacterial, antioxidant and antitumor activities due to the presence of annonaceous acetogenins, the expanding class of potential long-chain fatty acid which were initially noticed only in this species [23]. Significant interest in the studies of its derivatives present in the seeds of the plant also points to their remarkable anti-tumour and pesticidal activities [24]. Biosynthesis of AgNPs using the seed extract of *A. squamosa*, its characterization and biological activity assay has been done in this study. Present approach for the synthesis of AgNPs using a waste part of the plant material has economic and environmental benefits compared to conventional chemical or physical methods of nanoparticle synthesis. As reported in other

plant-mediated synthesis of silver nanoparticles, the phytochemicals act as capping and stabilizing agent, can enhance the biological activity of the AgNPs [8].

Materials and methods

Sample preparation

The fruits of *Annona squamosa* L. were procured from Thrissur, Kerala, India (Fig. 1). The plant was identified with the help of Flora of the Presidency of Madras [25]. The seeds were separated from the fruit and oven dried. Finely ground seeds of *A. squamosa* (20 g) were boiled with 200 mL of distilled water to prepare the aqueous extract. The filtrate of the extract was further centrifuged at 2000 rpm for 10 min and the extract was stored in amber coloured reagent bottles at 4 °C for further use.

Synthesis of silver nanoparticles

Silver nitrate solution (100 mL, 1 mmol) was added to a beaker containing 10 mL of the seed extract and mixed well. The reaction mixture was kept under different physical conditions such as at room temperature, at 60 °C, sunlight and ultraviolet lamp (30 W, 253 nm, Philips Holland). When the solution was kept under sunlight for 30 min, the colour of the mixture changed to yellowish-brown and later to reddish-brown.

Characterization of AgNPs

UV–Visible analysis

To monitor the complete bioreduction of AgNO₃ to silver nanoparticles, 1 mL of the sample suspension was diluted with 2 mL of distilled water and the spectrum of this sample was recorded using UV–Visible



Fig. 1 Fruit and seed of *Annona squamosa* L.

spectrophotometer (Shimadzu UV probe 1800) in the scanning range 200–700 nm having a resolution of 1 nm.

FT-IR analysis

The seed extract (10 mL) was added to 100 mL AgNO₃ (1 mmol) and kept under sunlight with continuous stirring. After 30 min exposure, it was centrifuged at 14,000 rpm (High speed-refrigerated-centrifuge, Thermo Electron LED, Germany) for 20 min. The pellet was suspended in distilled water, centrifuged twice and allowed to dry in a hot air oven. The AgNPs thus obtained were used for FT-IR and XRD analysis.

FT-IR analysis of the dried AgNPs was carried out using potassium bromide (KBr) pellet method. The spectrum was recorded using Fourier transform infrared spectrometer (Parkin-Elmer Pvt Ltd.) equipped with JASCO IRT-7000 Intron Infrared Microscope in transmittance mode operating at a resolution of 4 cm⁻¹.

XRD analysis

PANalytical X-ray diffractometer at a scanning rate of 20 min⁻¹ with an operating voltage of 40 kV, monochromatic filter in the 2θ range 10–80, was used in the present study. It was used to examine phase identification and characterization of the crystal structure of the nanoparticles.

TEM analysis

Transmission electron microscopy (TEM) technique was used to visualize the morphology and size of the synthesized AgNPs. The 200 kV ultra-high resolution transmission electron microscope (JEOL, JEM 2100 h with EELS) was used. TEM grids were prepared by placing 5 μL of the as-synthesized AgNP solutions on carbon-coated copper grids and dried under the lamp.

Biological activity of AgNPs

Photocatalytic degradation of toxic dye

Coomassie Brilliant Blue (CBB) is a member of triphenylmethane dyes that were developed for use in the textile industry but are now commonly used for staining proteins in analytical biochemistry. A freshly prepared solution (1 mL) containing silver nitrate and the plant extract (ratio 10:1) was added to 5 mL of 1% CBB solution with stirring and kept under sunlight. At specific time intervals (10, 20, 30 min), 2 mL of the solution was taken and the absorbance (480–680 nm) was recorded.

Antibacterial assay

Nutrient agar media (25 mL, Hi-Media, Mumbai) was poured into petriplates under sterile conditions and left to solidify at room temperature. The culture suspensions from pure cultures of Gram-positive bacteria *Staphylococcus aureus* (MTCC96) and Gram-negative bacteria *Klebsiella pneumoniae* (MTCC109) were chosen based on their clinical and pharmacological importance [26]. The bacterial strains were obtained from the Institute of Microbial Technology, Chandigarh, India. Antibacterial activities of AgNPs against these two bacterial strains were investigated by agar disc diffusion method [27]. The sterile filter paper discs (6 mm diameter) were saturated with 30 μL each of 100 μg/mL of AgNPs, 0.1 g/mL of the plant extract (negative control) and tetracycline disc (positive control) with demineralised water as solvent. The filter paper discs were placed equidistantly on the inoculated media and diffusion of the solution was allowed to occur for 30 min at room temperature. Plates were then inverted and incubated at 37 °C for 24 h. Triplicates were employed per treatment and the average zone of inhibition was recorded. Significance levels of standard and treatments were compared with one way ANOVA test using SPSS 20.0 software.

Larvicidal bioassay

Anopheles stephensi mosquitos were reared in the vector control laboratory, Kerala Veterinary and Animal Sciences University, Thrissur, Kerala, India. The larvae were fed on dog biscuits and yeast powder in 3:1 ratio. Adults were fed blood through a parafilm. Mosquitoes were held at 28 ± 2 °C temperature and 70–85% relative humidity with a 12 h light/12 h dark photoperiod. Larvicidal activity of the biogenic AgNPs was evaluated according to WHO protocol [28]. Five replicates having 100 larvae each of late III and early IV instar stages were used for bioassays. Five concentrations of AgNPs (12, 24, 36, 48 and 60 μg/mL) and water control replicates were run simultaneously. The number of dead and alive larvae in the replicates was recorded after 24 h and the results were expressed as percent mortality. The lethal concentrations that kill 50 percent of the treated larvae (LC 50) and 90 percent of the treated larvae (LC 90) were calculated [29]. The average larval mortality data were subjected to probit analysis for calculating LC 50 and LC 90 at 95% of upper confidence limit and lower confidence limit. Chi-squared values were calculated using SPSS 20.0 software.

Phytotoxicity assay

Germination test was performed using chickpea (*Cicer arietinum*) seeds. 50 surface-sterilized seeds were kept on

moist filter papers soaked in the respective treatment solution (25%, 50%, 75% and 100% v/v of AgNP dispersions) in sterilized petriplates and were incubated in dark at 25 °C. Seeds with root tip 1 mm and higher were considered as germinated. The length of root and shoot (in mm) obtained following 72 h after the germination of seeds was observed and percent germination was calculated thereafter.

Results and discussion

Synthesis of silver nanoparticles

Reduction of AgNO₃ to silver nanoparticles took place when the aqueous seed extract of *A. squamosa* was added to 1 mmol silver nitrate solution. Formation of AgNPs was indicated by the colour change of the solution to deep reddish-brown when the solution was exposed to sunlight for 30 min (Fig. 2a). The solution kept at 30 °C (rt), 60 °C or under UV lamp showed only light yellow colour even after 24 h of exposure. AgNPs appeared to be reddish-brown in the aqueous medium as a result of surface plasmon vibrations.

Characterization of AgNPs

Characterization of the AgNPs has been done using UV–Visible spectroscopy, Fourier transform infrared spectrophotometer, X-ray diffractometer, and Transmission electron microscope. These techniques help to monitor the shape, size, surface area, and crystalline structure of nanoparticles.

UV–Visible analysis

Absorption spectra of AgNPs formed in the reaction media after 30 min from the initiation of the reaction have an absorption maximum in the range 420–450 nm due to surface plasmon resonance (SPR) of AgNPs (Fig. 2b) [30]. Secondary metabolites such as fatty acids and polyphenols present in the seed extract is responsible for the reduction of silver nitrate to silver nanoparticles. Previous studies have reported that the seeds of *A. squamosa* can be used as a potential candidate in pharmacological preparations due to their bioactive secondary metabolites [31]. The broadening of the peak also indicated the formation of polydispersed nanoparticles [32].

FT-IR analysis

Prominent bands of absorbance in FT-IR spectra (Fig. 3) were observed at 1096, 1232, 1319, 1386, 1636, 2208, 3400 cm⁻¹. These peaks represent respectively ether linkage, C–N, O–H bending, aliphatic and aromatic –C=C–, amide,

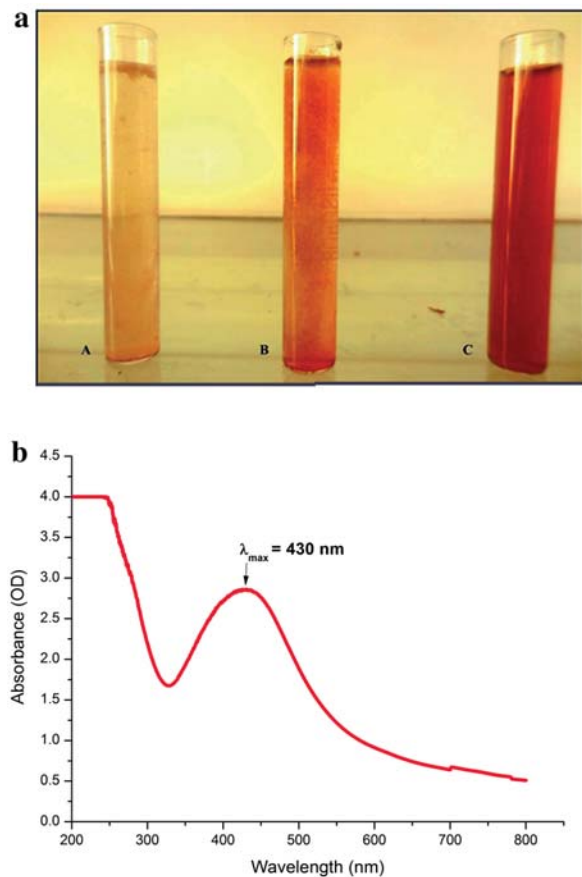


Fig. 2 a Colour change during the formation of AgNPs. b UV–Vis spectrum

alkynic and phenolic or alcoholic groups present in the phytochemicals. The FT-IR analysis confirms the capping over AgNPs with plant-derived secondary metabolites. These capped AgNPs helped to enhance the stability of AgNPs in colloidal solution by preventing aggregation of particles. Since they are capped by biomolecules they may serve as a better candidate for the drug delivery systems [33]. Synthesis of nanoparticles using plant extracts can potentially eliminate the problem of chemical agents for nanoparticle capping, which may have adverse effects in its application, thus making plant-derived nanoparticles more compatible.

XRD analysis

XRD pattern of the biosynthesized AgNPs showed two intense peaks in the spectrum with 2θ values ranging from 20 to 80 (Fig. 4). XRD spectra of pure crystalline silver structures have been published by the Joint Committee on Powder Diffraction Standards (File no.04-0783). A comparison of the XRD spectrum with the standard confirmed

Fig. 3 IR spectrum of AgNPs synthesised using *Annona squamosa* L. seed extract

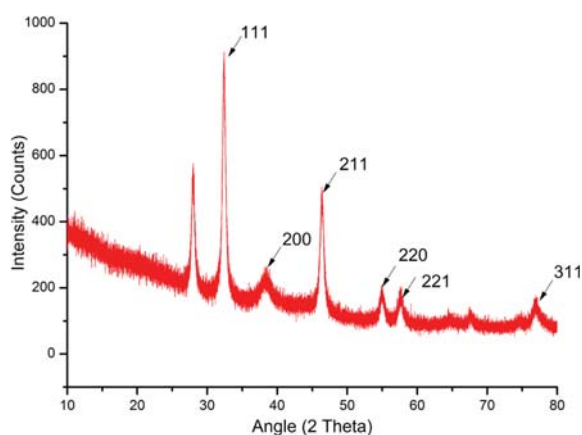
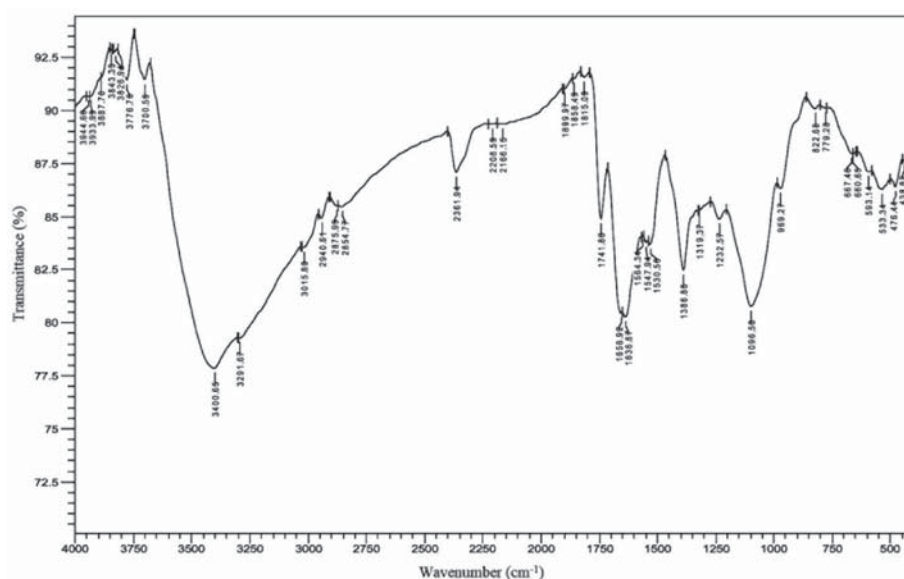


Fig. 4 XRD pattern of the silver nanoparticles

that the silver particles formed in our experiments were in the crystalline phase. The peaks at 2θ values 31.55° and 45.63° can be indexed respectively as 111, 200 planes of face-centred cubic silver. The Bragg reflections corresponding to (111) sets of lattice planes were observed which may be indexed based on the face-centred cubic structure of silver. The XRD pattern thus clearly indicated that the silver nanoparticles were crystalline. The other peaks having 2θ values at 27.17° , 35.36° , 53.65° and 56.81° are due to the coexistence of organic compounds accompanying crystalline AgNPs. Such unidentified crystalline peaks are apparent in many works in which the XRD pattern includes the relevant 2θ range [34].

TEM analysis

Nanoparticle composition and size distribution could be visualized through the Transmission electron microscope. The TEM images of AgNPs obtained in the present study are shown in Fig. 5. TEM image explained the size and shape of the silver nanoparticles. The particle size of AgNPs showed a size range 14–28 nm. The average particle size observed is 22 ± 5 nm. Furthermore, the analysis demonstrated that the AgNPs were polycrystalline with irregular spherical shapes and narrow size distribution. Energy-dispersive X-ray spectroscopy (EDAX) analysis of the AgNPs showed a high-pitched absorption peak at 2.5 keV inferring the existence of metallic silver (Fig. 5c). Elements from the plant residue as well as residual copper from copper grid account for the rest of the peaks in the spectrum. AgNPs prepared using plant extracts are stable in solution up to 4 weeks after its synthesis due to the presence of a thin layer of organic material surrounding the nanoparticles. This is one of the advantages of nanoparticles synthesised using plant extract than the ones which were synthesised using chemical methods.

Biological activity assay of AgNPs

The unique properties of silver nanoparticles have been investigated for dye degradation, antimicrobial applications, larvicidal activities and phytotoxicity assay.

Photocatalytic degradation of toxic dye

Silver nanoparticles and their composites showed greater catalytic activity towards dye degradation and its removal.

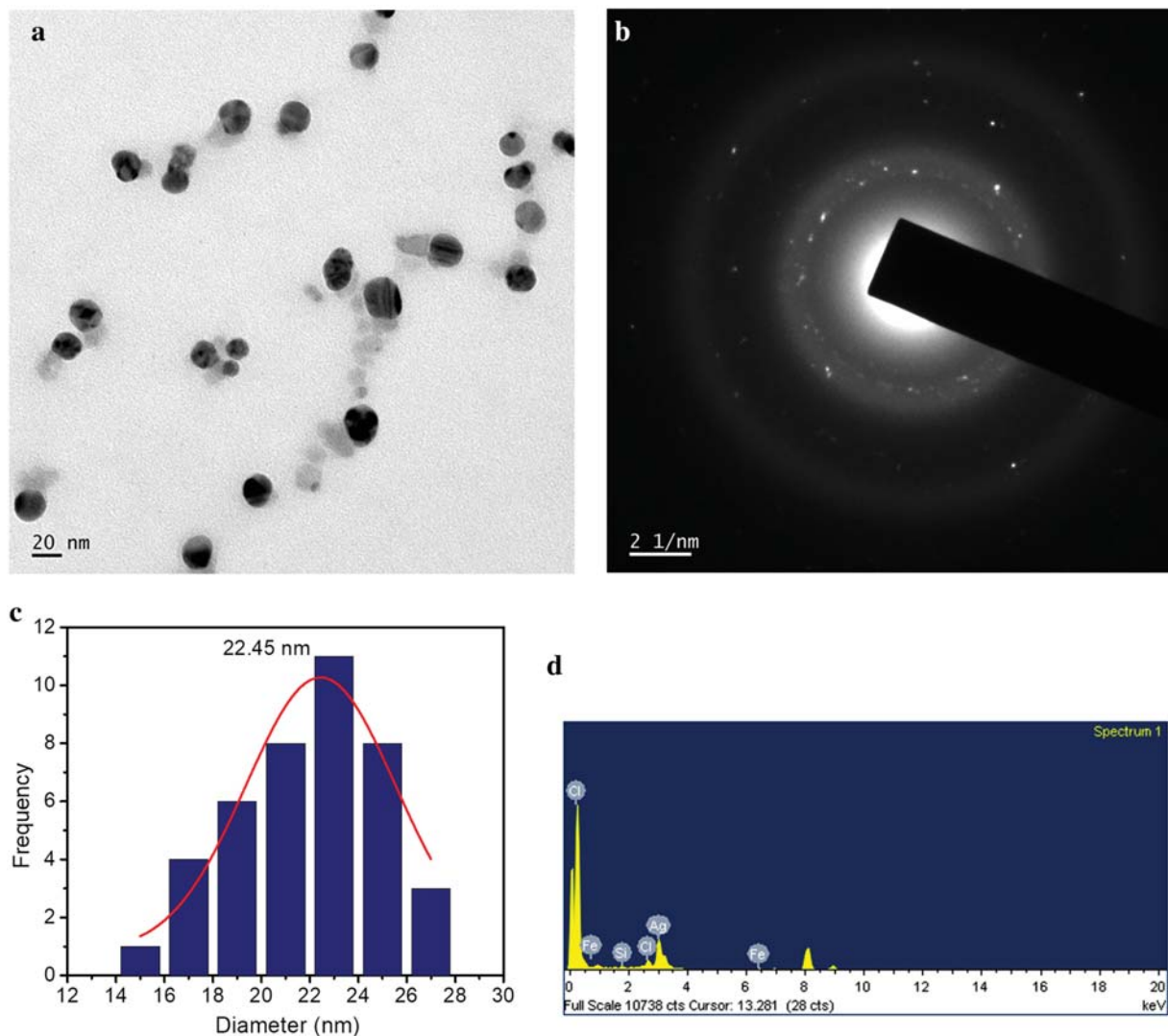


Fig. 5 a TEM image b SAED pattern and c particle size distribution histogram and d EDAX image of AgNPs

In the present study, the surface plasmon resonance (SPR) band of CBB–AgNPs solution was observed at 430 nm which became apparent after 10 min of mixing CBB with silver nitrate and the plant extract (ratio 10:1). The absorption at 430 nm is due to the formation of metallic silver nanoclusters and its intensity increases with time. This hyperchromic shift is due to the increase in the number of nanoparticles formed by the reduction of silver ions present in the aqueous solution. The peak corresponding to CBB observed around 580 nm disappeared completely within 30 min indicating the photocatalytic degradation of Coomassie Brilliant Blue (Fig. 6).

Antibacterial assay

Silver nanoparticles have been extensively studied in recent years due to their antibacterial and therapeutic potential. They can create reactive oxygen species which cause irreversible damage to bacteria and also have a strong affinity in binding to DNA or RNA which interferes with the microbial replication process [35]. In this study, the antimicrobial property of AgNPs was investigated against *Klebsiella pneumoniae* (Gram negative) and *Staphylococcus aureus* (Gram positive) by disc diffusion method under sterilized conditions using Tetracyclin as positive control (Fig. 7).

Fig. 6 UV–Vis spectra of CBB dye degradation using the AgNPs

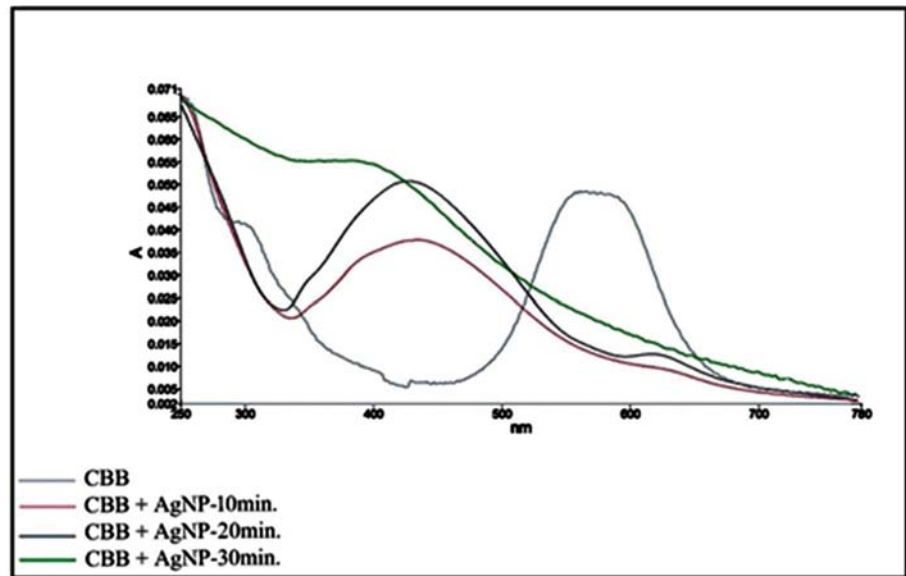
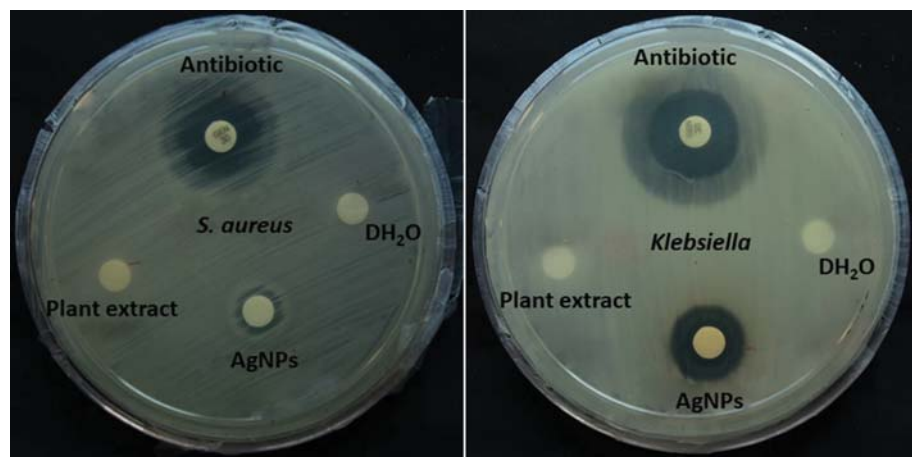


Fig. 7 Antibacterial study of AgNPs



Triplicates were employed per treatment and the average zone of inhibition was recorded. Significance levels of standard and treatments were compared by independent sample *t* test using SPSS 20.0 software (Table 1).

From the table, it is clear that, in the case of *S.aureus*, the area of the inhibition zone corresponding to AgNPs is not significantly different from that of Tetracyclin; but it is significantly different from that of the plant extract. Positive value of the test statistic (9.35) indicates that the area corresponding to AgNPs is significantly larger than that of the plant extract. Similarly, the area of the inhibition zone corresponding to plant extract is significantly smaller than that of Tetracyclin. In the case of *K.pneumoniae*, area of the inhibition zone corresponding to AgNPs is significantly different from that of Tetracyclin and the plant extract. Positive values of the test statistics (63.25 and 49.68) indicate that the area corresponding to AgNPs is significantly larger than that of

Table 1 Inhibitory effects of AgNs against pathogenic microorganisms

Bacterial isolate	Treatments	Mean*	SD	Test statistic
<i>S.aureus</i>	AgNPs	13	1.62	1.56
	Tetracyclin (control)	11	0.81	
	AgNPs	18	0.12	9.35*
	Plant extract	4	0.38	
	Plant extract	2	0.38	-14.23*
<i>K.pneumoniae</i>	Tetracyclin (control)	11	0.81	
	AgNPs	18	0.12	63.25*
	Tetracyclin (control)	12	0.06	
	AgNPs	18	0.12	49.68*
	Plant extract	4	0.38	
	Plant extract	4	0.38	-29.41*
	Tetracyclin (control)	12	0.06	

*Values corresponding to three replicates

Test statistic in bold indicate that the values are significant

Tetracyclin and the plant extract. As in the case of *S.aureus*, area of the inhibition zone corresponding to plant extract is significantly smaller than that of Tetracyclin. AgNPs produced a maximum zone of inhibition against both bacterial strains when compared with positive control. Among the gram strains, the highest zone of inhibition occurred in gram-negative bacteria. This might be due to the presence of a thin peptidoglycan layer in gram-negative strain, allowing the easy penetration of silver nanoparticles, can bind to the sulphur and phosphorous atom of deoxyribonucleic acid [36, 37]. The antibacterial activity of AgNPs was found to be efficient compared to commercial antibiotic tetracycline.

Larvicidal bioassay

Silver nanoparticles synthesized using seed extract of *A. squamosa* were also tested for their activity against mosquito larvae. Larvicidal bioassays were performed against III and IV instars of *Anopheles stephensi* (Fig. 8).

Considerable mortality was evident after the treatment of silver nanoparticle solution for the two important larval stages of the vector mosquito, *Anopheles stephensi*. Mosquito larvae at III instar stage showed 100 percent mortality in bioassays with AgNPs at 60 µg/mL. The LC50 and LC90 of III instars were the lowest (LC50 22.44 µg/mL and LC90 40.65 µg/mL), while that of IV instars was highest (LC50 27.83 µg/mL and LC90 48.92 µg/mL). The control showed nil mortality in the concurrent assay. χ^2 value was significant at $p \leq 0.05$ level (Table 2). Mechanism of the larvicidal activity of AgNPs can be attributed to the penetration of AgNPs into the insect gut wall followed by binding to phosphorous and sulfur group of deoxyribonucleic acid which eventually affect cellular function leading to cell death [38]. Routine use of synthetic insecticidal products for mosquito controlling disturbs the biological system and cause resurgences in mosquito populations. The prospect of utilising plants for synthesizing silver nanoparticles and testing their efficacy in controlling mosquito larvae is an approach facilitating

Fig. 8 Effect of AgNPs against III and IV instars of *Anopheles stephensi*



Table 2 Dose-dependent larvicidal activity of silver nanoparticles synthesized from *A. squamosa* seed extract against 3rd and 4th instars of mosquito larvae

Larval stage	Concentration (µg/mL)	Mortality (%) ± SD	LC ₅₀ (µg/mL)	LCL-UCL	LC ₉₀ (µg/mL)	LCL-UCL	χ^2
3rd Instar	60	100 ± 0.0	22.44	16.25–28.30	40.65	33.69–54.73	18.881*
	48	84.2 ± 0.6					
	36	66.7 ± 1.5					
	24	45.2 ± 2.2					
	12	29.3 ± 1.2					
	Control	0.0 ± 0.0					
4th Instar	60	95.3 ± 1.2	27.83	21.67–34.46	48.92	40.73–66.06	17.428*
	48	71.4 ± 0.8					
	36	50.2 ± 1.4					
	24	32.7 ± 0.2					
	12	23.5 ± 1.5					
	Control	0.0 ± 0.0					

SD standard deviation, LCL lower confidence limit, UCL upper confidence limit, χ^2 chi-square test

* $p < 0.05$, level of significance

Values are mean ± SD of five replicates

Table 3 Impact of AgNPs on shoot length of chickpea seeds

Concentration of AgNPs (%)	Length of shoot (Mean \pm SE) (mm)	
	After 48 h	After 72 h
100	1.94 \pm 0.02	6.92 \pm 0.03
75	1.41 \pm 0.00	2.94 \pm 0.02
50	1.40 \pm 0.00	2.95 \pm 0.01
25	1.39 \pm 0.01	4.92 \pm 0.03
0	2.92 \pm 0.03	4.97 \pm 0.00

Table 4 Impact of AgNPs on root length of chickpea seeds

Concentration of AgNPs (%)	Length of root (Mean \pm SE) (mm)	
	After 24 h	After 48 h
100	9.82 \pm 0.04	29.84 \pm 0.07
75	6.99 \pm 0.00	14.91 \pm 0.03
50	6.01 \pm 0.01	8.92 \pm 0.01
25	5.02 \pm 0.02	7.94 \pm 0.02
0	5.97 \pm 0.04	20.02 \pm 0.02

the development of a more potent and environmentally safe biopesticide.

Phytotoxicity assay

Toxicity analysis of the AgNPs was carried out on Chickpea (*Cisus arietinum*) seeds and their resultant root and shoot lengths were recorded. Seeds were considered to have germinated by observing the emergence of radicles. Results obtained varied significantly with each treatment. Shoot length and root length of seedlings (Tables 3, 4; Fig. 9b, c) increased significantly in a dose-dependent manner, with a marked increase in seeds treated with 100% AgNP solution. The germination of chickpea seeds treated with 100% AgNP solution was significantly higher than those treated with a low concentration of AgNP solution and control (Table 5; Fig. 9a). The surface coating of AgNPs, their aggregation state and the release of dissolved silver are related to the toxicity of AgNPs. Studies have reported that compared to PVP-coated AgNPs, citrate-coated AgNPs were toxic to freshwater organisms [39]. Hence the increased growth and germination of chickpea seeds could be attributed to the biomolecules of *Annona squamosa* seed extract coated over the synthesized AgNPs. Therefore the biosynthesized AgNPs showed low toxicity and improved plant growth.

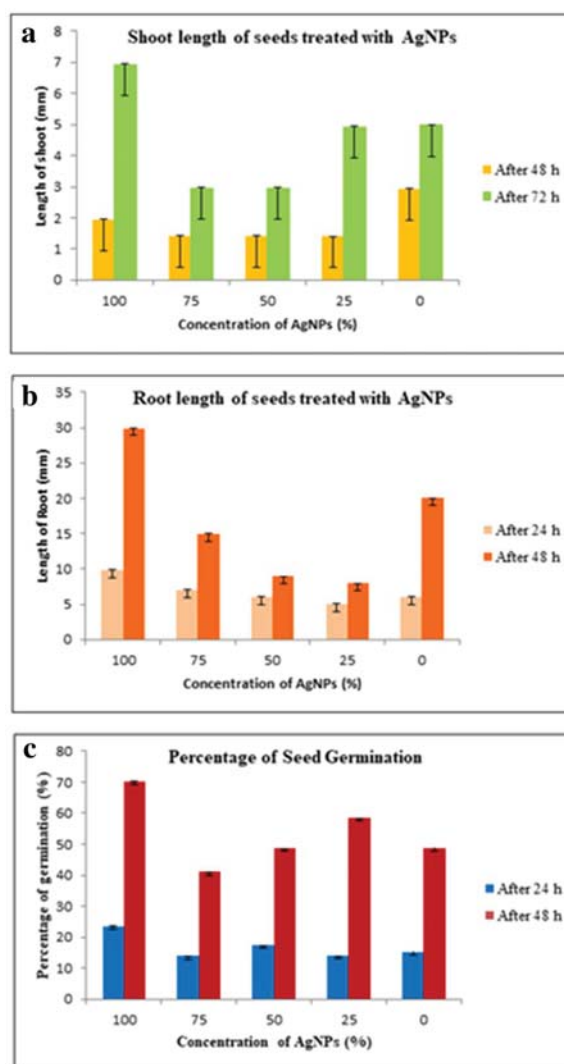

Fig. 9 Impact of AgNPs on chickpea, **a** seed germination, **b** root length and **c** shoot length

Table 5 Impact of AgNPs on chickpea seed germination

Concentration of AgNPs (%)	Percentage of seed germination (Mean \pm SE) (%)	
	After 24 h	After 48 h
100	23.6 \pm 0.02	70.18 \pm 0.04
75	13.9 \pm 0.00	41.00 \pm 0.01
50	17.37 \pm 0.01	48.62 \pm 0.03
25	13.91 \pm 0.00	58.4 \pm 0.01
0	15.28 \pm 0.01	48.67 \pm 0.01

Conclusion

Green methods for nanoparticle synthesis are attractive due to their importance in human health and environment. In the present study, we demonstrated that *Annona squamosa* L. seed extract can act as a reducing agent to generate AgNPs via a green approach. The synthesis of AgNPs was confirmed using UV–Visible spectroscopy with an absorption maximum at 430 nm. FT-IR spectrum revealed the presence of phytochemicals which is responsible for efficient capping and stabilization of the nanoparticles. XRD pattern demonstrated the polycrystalline nature of AgNPs. HR-TEM image showed its size distribution in the range 14–28 nm and spherical morphology. Moreover, biological assay indicated that AgNPs could be used as antibacterial, larvicidal and seed growth-promoting agent. The nanoparticles exhibited good photocatalytic activity towards the degradation of coomassie brilliant blue (CBB) dye ultimately formulating a bioremediation protocol. Formulation of optimal dosage of AgNP based herbal nanolarvicide for the control of vector borne diseases is a need of the hour. The present study act as a baseline for the preparation and application of valuable nanomedicines in future.

Declarations

Conflict of Interest The authors declare no conflict of interest.

References

- Korkmaz N, Ceylan Y, Karadağ A, Bülbül AS, Aftab MN, Saygili S, Şen F (2020) Biogenic silver nanoparticles synthesized from *Rhododendron ponticum* and their antibacterial, antibiofilm and cytotoxic activities. *J Pharm Biomed Anal* 179:112993
- Pourzahedi L, Vance M, Eckelman M (2017) Life cycle assessment and release studies for 15 nanosilver-enabled consumer products: investigating hotspots and patterns of contribution. *Environ Sci Technol* 51:7148–7158
- Ahmed S, Ahmad M, Swami BL, Ikram S (2016) A review on plants extract mediated synthesis of silver nanoparticles for antimicrobial applications: a green expertise. *J Adv Res* 7:17–28
- Chung I-M, Park I, Seung-Hyun K, Thiruvengadam M, Rajakumar G (2016) Plant-mediated synthesis of silver nanoparticles: their characteristic properties and therapeutic applications. *Nanoscale Res Lett* 11:40
- Guzman M, Dille J, Godet S (2012) Synthesis and antibacterial activity of silver nanoparticles against gram-positive and gram-negative bacteria. *Nanomed Nanotechnol Biol Med* 8:37–45
- Korkmaz N, Ceylan Y, Hamid A, Karadağ A, Bülbül AS, Aftab MN, Cevik O, Sen F (2020) Biogenic silver nanoparticles synthesized via *Mimusops elengi* fruit extract, a study on antibiofilm, antibacterial, and anticancer activities. *J Drug Deliv Sci Technol* 59:101864
- Korkmaz N, Ceylan Y, Karadağ A, Bülbül AS, Aftab MN, Saygili S, Sen F (2020) Biogenic silver nanoparticles synthesized from *Rhododendron ponticum* and their antibacterial, antibiofilm and cytotoxic activities. *J Pharm Biomed Anal* 179:112993
- Gopinath SM, Saha NS, John J, Khanum NS, Ganesh S, Patil A (2013) Biological synthesis characterization and application of silver nano particles a review. *Int J Pharm Appl* 4:19–28
- Korkmaz N, Ceylan Y, Taslimi P, Karadağ A, Bülbül AS, Sen F (2020) Biogenic nano silver: synthesis, characterization, antibacterial, antibiofilms, and enzymatic activity. *Adv Powder Technol* 31:2942–2950
- Korkmaz N (2020) Bioreduction, the biological activity, characterization and synthesis of silver nanoparticles. *Turkish J Chem* 44:325–334
- McFarland AD, Van Duyne RP (2003) Single silver nanoparticles as real-time optical sensors with zeptomole sensitivity. *Nano Lett* 3:1057–1062
- Marimuthu S, Antonisamy AJ, Malayandi S, Rajendran K, Tsai PC, Pugazhendhi A, Ponnusamy VK (2020) Silver nanoparticles in dye effluent treatment: a review on synthesis, treatment methods, mechanisms, photocatalytic degradation, toxic effects and mitigation of toxicity. *J Photochem Photobiol B Biol* 205:111823–111826
- Radinia IA, Hasan N, Malik MA, Khan Z (2018) Bio-based synthesis of magnetic nanoparticles and their applications. *J Photochem Photobiol B* 183:154–163
- Kumar P, Govindaraju M, Senthamilselvi S, Premkumar K (2013) Photocatalytic degradation of methyl orange dye using silver (Ag) nanoparticles synthesized from *Ulva lactuca*. *Colloids Surf B* 103:658–661
- Marimuthu S, Rahuman AA, Rajakumar G, Santhoshkumar T, Kirthi AV, Jayaseelan C, Bagavan A, Zahir AA, Elango G, Kamaraj C (2011) Evaluation of green synthesized silver nanoparticles against parasites. *Parasitol Res* 108:1541–1549
- Sivapriyajothi S, Kumar PM, Kovendan K, Subramaniam J, Murugan K (2014) Larvicidal and pupicidal activity of synthesized silver nanoparticles using *Leucas aspera* leaf extract against mosquito vectors, *Aedes aegypti* and *Anopheles stephensi*. *J Entomol Acarol Res* 46:77–84
- Bhuvaneshwari R, Xavier RJ, Arumugam M (2016) Larvicidal property of green synthesized silver nanoparticles against vector mosquitoes (*Anopheles stephensi* and *Aedes aegypti*). *J King Saud Univ Sci* 28:318–323
- Anil Kumar V, Ammani K, Jobina R, Parasuraman P, Siddhardha B (2016) Larvicidal activity of green synthesized silver nanoparticles using *Excoecaria agallocha* L. (Euphorbiaceae) leaf extract against *Aedes aegypti*. *IET Nanobiotechnol* 10:382–388
- Velayutham K, Rahuman AA, Rajakumar G, Roopan SM, Elango G, Kamaraj C, Siva C (2013) Larvicidal activity of green synthesized silver nanoparticles using bark aqueous extract of *Ficus racemosa* against *Culex quinquefasciatus* and *Culex gelidus*. *Asian Pac J Trop Med* 6:95–101
- Gupta SD, Agarwal A, Pradhan S (2018) Phytostimulatory effect of silver nanoparticles (AgNPs) on rice seedling growth: an insight from antioxidative enzyme activities and gene expression patterns. *Ecotoxicol Environ Saf* 161:624–633
- Gajalakshmi S, Divya R, Deepika VD, MythiliSathivelu SA (2011) Pharmacological activities of *Annona squamosa*; a review. *Int J Pharm Sci Rev Res* 10:24–29
- Shirwaikar A, Rajendran K, Kumar CD, Bodla R (2004) Anti-diabetic activities of aqueous leaf extract of *Annona squamosa* in streptozotocin–nicotinamide type 2 diabetic rats. *J Ethnopharmacol* 91:171–175
- Alali FQ, Liu X-X, McLaughlin JL (1999) Annonaceous acetogenins: recent progress. *J Nat Prod* 62:504–540

24. Biba VS, Jeba MPW, Remani P (2013) Differential effects of *Annona Squamosa* seed extracts: antioxidant, antibacterial, cytotoxic and apoptotic study. *Int J Pharm Biol Sci* 4:899–907
25. Gamble JS (1935) The flora of the presidency of Madras. Adlard & Son Ltd, London
26. McCracken WA, Cowsan RA (1983) Clinical and oral microbiology. Hemisphere Publishing Corporation, New York, p 512
27. Rios JL, Recio MC, Villar A (1988) Screening methods for natural products with antimicrobial activity: a review of the literature. *J Ethnopharmacol* 23:127–149
28. WHO (1992) Lymphatic filariasis: the disease and its control. 5th report. Who expert committee on filariasis. Technical Report Series p 821
29. Finney DJ (1971) Probit analysis, vol 551. Cambridge University Press, London, pp 68–72
30. Amendola V, Bakr OM, Stellacci F (2010) A study of the surface plasmon resonance of silver nanoparticles by the discrete dipole approximation method: effect of shape, size, structure, and assembly. *Plasmonics* 5:85–97
31. Zahid M, Arif M, Rahman MA, Singh K, Mujahid M (2018) Solvent extraction and gas chromatography-mass spectrometry analysis of *Annona squamosa* L. seeds for determination of bioactives, fatty acid/fatty oil composition, and antioxidant activity. *J Diet suppl* 15:613–623
32. Fatimah I (2016) Green synthesis of silver nanoparticles using extract of *Parkia speciosa* Hassk pods assisted by microwave irradiation. *J Adv Res* 7:961–969
33. Barman SR, Nain A, Jain S, Punjabi N, Mukherji S, Satija J (2018) Dendrimer as a multifunctional capping agent for metal nanoparticles for use in bioimaging, drug delivery and sensor applications. *J Mater Chem B* 6:2368–2384
34. Sands DE (1993) Introduction to crystallography. Dover, New York, p 51
35. Harrison JJ, Tremaroli V, Stan MA, Chan CS, Vacchi-Suzzi C, Heyne BJ, Parsek MR, Ceri H, Turner RJ (2009) Chromosomal antioxidant genes have metal ion-specific roles as determinants of bacterial metal tolerance. *Environ Microbiol* 11:2491–2509
36. Dakal TC, Kumar A, Majumdar RS, Yadav V (2016) Mechanistic basis of antimicrobial actions of silver nanoparticles. *Front Microbiol* 7:1831
37. Qing Y, Cheng L, Li R, Liu G, Zhang Y, Tang X, Wang J, Liu H, Qin Y (2018) Potential antibacterial mechanism of silver nanoparticles and the optimization of orthopedic implants by advanced modification technologies. *Int J Nanomed* 13:3311–3327
38. Kumar D, Kumar P, Singh H, Agrawal V (2020) Biocontrol of mosquito vectors through herbal-derived silver nanoparticles: Prospects and challenges. *Environ Sci Pollut Res* 27:25987–26024
39. Rani PU, Yasur J, Loke KS, Dutta D (2016) Effect of synthetic and biosynthesized silver nanoparticles on growth, physiology and oxidative stress of water hyacinth: *Eichhornia crassipes* (Mart) Solms. *Acta Physiol Plant* 38:1–9

Publisher's Note Springer Nature remains neutral with regard to jurisdictional claims in published maps and institutional affiliations.